Sawamura D, Yasukawa K, Kodama K, Yokota K, Sato-Matsumura KC, Tanaka T, Shimizu H (2002) The majority of keratinocytes incorporate intradermally injected plasmid DNA regardless of size but only a small proportion of cells can express the gene product. J Invest Dermatol 118:967–971

Sawamura D, Goto M, Yasukawa K, Sato-Matsumura K, Nakamura H, Ito K, Nakamura H, Tomita Y, Shimizu H (2005) Genetic studies of 20 Japanese families of dystrophic epidermolysis bullosa. J Hum Genet 50:543–546

Shimizu H, McGrath JA, Christiano AM, Nishikawa T, Uitto J (1996) Molecular basis of recessive dystrophic epidermolysis bullosa genotype/phenotype correlation in a case of moderate clinical severity. J Invest Dermatol 106:119–124

Shimizu H, Hammami-Hauasli N, Hatta N, Nishikawa T, Bruckner-Tuderman L (1999) Compound heterozygosity for silent and dominant glycine substitution mutations in COL7A1 leads to a marked transient intracytoplasmic retention of procollagen VII and a moderately severe dystrophic epidermolysis bullosa phenotype. J Invest Dermatol 113:419–421

Uitto J, Chung-Honet LC, Christiano AM (1992) Molecular biology and pathology of type VII collagen. Exp Dermatol 1:2–11

Wessagowit V, Ashton GH, Mohammedi R, Salas-Alanis JC, Denyer JE, Mellerio JE, Eady RA, McGrath JA (2001) Three cases of de novo dominant dystrophic epidermolysis bullosa associated with the mutation G2043R in *COL7A1*. Clin Exp Dermatol 26:97–99

J. Biochem. **139**, 399–406 (2006)
doi:10.1093/jb/mvj042

Identification and Characterization of a Neutralizing Monoclonal Antibody for the Epitope on HM-1 Killer Toxin

Dakshnamurthy Selvakumar[1], Qing-Zhu Zhang[1], Masahiko Miyamoto[1], Yasuhiro Furuichi[2] and Tadazumi Komiyama[1,*]

[1]Department of Biochemistry, Faculty of Pharmaceutical Sciences, Niigata University of Pharmacy and Applied Life Sciences, 5-13-2 Kamishinei-cho, Niigata 950-208; and [2]GeneCare Research Institute Co. Ltd., 200 Kajiwara, Kamakura 247-0063

Received November 28, 2005; accepted December 17, 2005

Killer toxin-neutralizing monoclonal antibody (nmAb-KT) against HM-1 killer toxin (HM-1) produced by yeast *Williopsis saturnus* var. *mrakii* IFO 0895 reduces both the killing and glucan synthase inhibitory activity of HM-1. nmAb-KT is classified as IgG1(κ) and has been shown to be ineffective against HYI killer toxin produced by the related yeast *W. saturnus* var. *saturnus* IFO 0117. To determine the epitope for nmAb-KT, overlapping peptides were synthesized from the primary structure of HM-1. nmAb-KT reacted with peptides P5 (^{33}NVHWMVTGGST^{43}), P6 (^{39}TGGSTDGKQG^{48}) and P7 (^{44}DGKQGCATIWEGS^{56}), which represent the middle region of the HM-1 sequence. P6 reacted most strongly with nmAb-KT. Combined analysis by immunoblotting, surface plasmon resonance (SPR) analysis and yeast growth inhibition assay showed that nmAb-KT recognizes a specific epitope within peptide P6. The K_d value of nmAb-KT against HM-1 and P6 were determined to be 5.48×10^{-9} M and 1.47×10^{-6} M by SPR analysis, respectively. These results strongly indicate that nmAb-KT binds to HM-1 at the sequence ^{41}GSTDGK^{46}, and not to HYI at the same position. The potential active site of HM-1 involved in the killing activity against sensitive yeast is discussed.

Key words: epitope identification, β-1, 3-glucan synthase, HM-1 killer toxin, neutralizing monoclonal antibody, SPR analysis.

Abbreviations: HM-1, HM-1 killer toxin; HYI, HYI killer toxin; nmAb-KT, HM-1 killer toxin neutralizing monoclonal antibody; SPR, surface plasmon resonance; ELISA, enzyme-linked immunosorbent assay; TBS, 20 mM Tris-HCl (pH 7.5) containing 150 mM NaCl; TBS-T, 20 mM Tris-HCl (pH 7.5) containing 150 mM NaCl and 0.05% Tween 20.

Several fungi, especially yeasts, can produce proteinaceous killer toxins that are lethal to other taxonomically related or unrelated sensitive microorganisms, and can represent a sophisticated biological mechanism of competition in natural ecosystems (*1*). Species of *Williopsis* (*2*, *3*) produce killer toxins that kill other sensitive yeast strains (*4–7*). HM-1 and HYI are strong yeast killer toxins produced by yeasts *W. saturnus* var. *mrakii* IFO 0895 and *W. saturnus* var. *saturnus* IFO 0117 (*5*, *6*), which were previously known as *Hansenula mrakii* and *H. saturnus*, respectively (*2*).

HM-1 belongs to the K9-killer toxin group (*4*), and consists of 88 amino acids, of which 10 are cysteine (*8*). It is inactivated by reducing agents, such as 2-mercaptoethanol and dithiothreitol, suggesting that S-S bonds forming tertiary structures maintain the structure and biological activity of HM-1 (*7*). HM-1 is stable against heat treatment (100°C, 10 min) and a wide range of pH values (pH 2.0–11.0). The isoelectric point of HM-1 is pH 9.1 and the molecular mass is calculated to be 9,500 daltons from the amino acid sequence (*8*). The three-dimensional structure of HM-1 has been determined by nuclear magnetic resonance spectroscopy (*9*), and the HM-1 gene has been cloned from chromosomal DNA of HM-1–producing yeasts (*10*).

HYI consists of 87 amino acids and its molecular mass is about 9,500 Da (*11*). The isoelectric point of HYI is pH 5.8, and it is stable when heated at 60°C for 1 h and at pH 5.0 to 8.0 at 30°C for 24 h (*6*). Most of these features of HYI are similar to HM-1 except the isoelectric point and local amino acid sequences. Amino acid homology predicts that HM-1 is larger than HYI by one amino acid that is absent from HYI, corresponding to position 43 in HM-1 (*11*). Although, HM-1 and HYI show a small local difference in primary structure, the overall homology is 87% (*10*, *11*), and the mechanism of killing action against sensitive yeasts by inhibiting β-1,3-glucan synthase activity is shared by the two toxins (*12*, *13*).

The killer-toxin neutralizing monoclonal antibody (nmAb-KT) binds HM-1 and neutralizes the yeast killing activity of HM-1 (*8*). However, we previously prepared the HM-1–specific monoclonal antibodies 1F1 and 4A2, which bind to HM-1, but they did not neutralize the yeast killing activity of HM-1 (*14*). In this study, we investigated the epitope of HM-1 recognized by nmAb-KT using various synthetic overlapping peptides of HM-1 and HYI. The binding affinities of nmAb-KT for HM-1, HYI, HM-1 peptides and HYI peptide were compared by the effect on yeast growth, immunoblot blot analsysis, sandwich

*To whom all correspondence should be addressed. Tel: +81-25-268-1223, Fax: +81-25-268-1230, E-mail: tkomiyam@niigata-pharm.ac.jp

enzyme–linked immunosorbent assay (ELISA) and surface plasmon resonance (SPR) analysis. The epitope of HM-1 recognized by nmAb-KT was clearly identified. We believe this is the first report of the binding characteristics and mapping of the epitope site of yeast killer toxins as characterized by SPR and dot blotting analysis.

MATERIALS AND METHODS

Materials—Affinity purified nmAb-KT was prepared from the hybridoma clone of 6207 (*8*), and polyclonal rabbit anti-serum against HM-1 was prepared by Technology Incubation & Transfer Ltd. (Saitama, Japan) and Nippon Bio-Test Laboratories, Inc. (Tokyo, Japan). Purified HM-1 and HYI were prepared in our laboratory as previously described (*6*, *11*, *13*, *15*). A mouse monoclonal antibody isotyping kit was purchased from Amersham Biosciences Co. Ltd., (Tokyo, Japan). Horseradish peroxidase–conjugated anti-mouse goat IgG and alkaline phosphatase conjugated anti-mouse goat IgG were obtained from Sigma (St. Louis, MO, USA). The BIAcore X system, CM5 sensor chip and amine coupling kit were the products of Biacore AB (Uppsala, Sweden). Peptides were synthesized by Sigma Genosys Co. Ltd., Japan. To identify the sequence of the epitope for nmAb-KT, thirteen synthetic overlapping HM-1 peptides (P1–P13) were prepared from the N-terminus of the primary structure of HM-1 (Table 1). In addition to these peptides, one HYI nanopeptide representing the amino acid sequence of positions 39–47 of HYI was synthesized. YPD medium consisted of 1% yeast extract and 2% each of peptone and glucose.

Antibody Isotyping—The isotyping of nmAb-KT was determined using an antibody isotyping kit according to the manufacturer's protocol. Briefly, an isotyping stick was incubated with 3 μg/ml of nmAb-KT in 20 mM Tris-HCl (pH 7.5) containing 150 mM NaCl (TBS) for 15 min at room temperature with agitation. The stick was washed with TBS containing 0.05% Tween-20 (TBS-T), and incubated with horseradish peroxidase–conjugated anti-mouse goat IgG for 15 min at room temperature with shaking. Then, 4-chloro-1-naphthol in cold methanol and 0.1% hydrogen peroxide were added to identify the isotyping of nmAb-KT.

Table 1. **Overlapping peptides used to determine the epitope for nmAb-KT.**

Peptide name	Peptide sequence
HM-1 peptides	
P1	^{1}GDGYLIMCKNCDPN^{14}
P2	^{9}KNCDPNTGSCDWQNWNT^{26}
P3	^{22}QNWNTCVGIGA^{32}
P4	^{27}CVGIGANVHWMV^{38}
P5	^{33}NVHWMVTGGST^{43}
P6	^{39}TGGSTDGKQG^{48}
P7	^{44}DGKQGCATIWEGS^{56}
P8	^{49}CATIWEGSGCVGRSTT^{64}
P9	^{60}GRSTTMCCPA^{69}
P10	^{65}MCCPANTCCN^{74}
P11	^{70}NTCCNINT^{77}
P12	^{73}CNINTGFYIRS^{83}
P13	^{78}GFYIRSYRRVE^{88}
HYI nanopeptide	^{39}TGESNGQQG^{47}

Numbering of the peptide is based on the HM-1 amino acid sequence. Overlapping residues are underlined. Numbering of the amino acid positions is from the N-terminal amino acid.

Killing Activity of HM-1 and HYI with nmAb-KT—The killing activities of the HM-1 and HYI proteins were measured using a liquid culture method described previously (*12*). Approximately 4×10^6 cells/ml of *Saccharomyces cerevisiae* A451 were incubated in YPD medium containing 15 μg/ml of nmAb-KT or 40 ng/ml of HM-1 or HYI, or nmAb-KT combined with HM-1 or HYI, at 30°C for 8 h. Yeast growth was measured by absorbance at 600 nm.

Preparation of Membrane Fractions of S. cerevisiae—Membrane fractions of *S. cerevisiae* were prepared by a method described previously (*16*) with some modifications. Cells of *S. cerevisiae* A451 in the mid-exponential phase and collected by centrifugation were washed with 1 mM ethylene diamine tetraacetate (EDTA) and suspended in breaking buffer consisting of 50 mM Tris-HCl (pH 7.5), 0.5 M NaCl, 1 mM EDTA and 1 mM phenylmethanesulfonyl fluoride. The cells were disrupted with glass beads by vortexing and centrifuged for 5 min at $1,000 \times g$ at 4°C. The supernatant was centrifuged at $100,000 \times g$ for 30 min at 4°C. The membrane fraction obtained was homogenized in membrane buffer consisting of 50 mM Tris-HCl (pH 7.5), 10 mM EDTA, 1 mM β-mercaptoethanol and 33% glycerol, and stored at –80°C.

Measurement of β-1,3-Glucan Synthase Activity—β-1,3-Glucan synthase assay was performed according to the method of Cabib and Kang (*16*). The reaction mixture consisted of 5 mM UDP-D-[*U*-^{14}C]glucose, 75 mM Tris-HCl (pH 7.5), 0.75% bovine serum albumin, 25 mM KF, 0.75 mM EDTA, 20 μM guanosine 5′-[γ-thio]triphosphate and 10 μl of the membrane fraction of *S. cerevisiae* in a total volume of 40 μl. The reaction was started by adding the membrane fraction, and the mixture was incubated at 30°C for 60 min. To measure the effect of nmAb-KT on β-1,3-glucan synthase activity, 15 μg/ml of nmAb-KT or 2 μg/ml of HM-1 or HYI, or nmAb-KT combined with HM-1 or HYI, was added before the addition of the membrane fraction. The reaction was stopped by adding cold 250 μl 10% trichloroacetic acid, and the mixture was incubated on ice for 10 min, and then filtered through glass microfibre filters (Whatman GF/B). The filters were washed four times with 250 μl of cold 10% trichloroacetic acid, and further washed twice with 250 μl 95% ethanol. The radioactivity retained on the filters was counted in a liquid scintillation counter.

Sodium Dodecyl Sulfate–Polyacrylamide Gel Electrophoresis (SDS-PAGE) and Western Blotting—The HM-1 and HYI proteins (each 0.1 μg) were separated in a 15% polyacrylamide gel by electrophoresis, and the proteins were transferred onto a ProBlott membrane (Applied Biosystem) using a semi-dry electroblotting apparatus. The membrane was blocked for 1 h in TBS-T supplemented with 4% non-fat dry milk, and then incubated for 2 h with 3 μg/ml of nmAb-KT in blocking solution. The membrane was washed three times with TBS-T, and then further incubated with alkaline phosphatase–conjugated anti-mouse goat IgG for 1 h. The membrane was washed and the proteins on the membrane were visualized by adding Western blue (Promega) as a substrate. A prestained broad range standard was used as a marker.

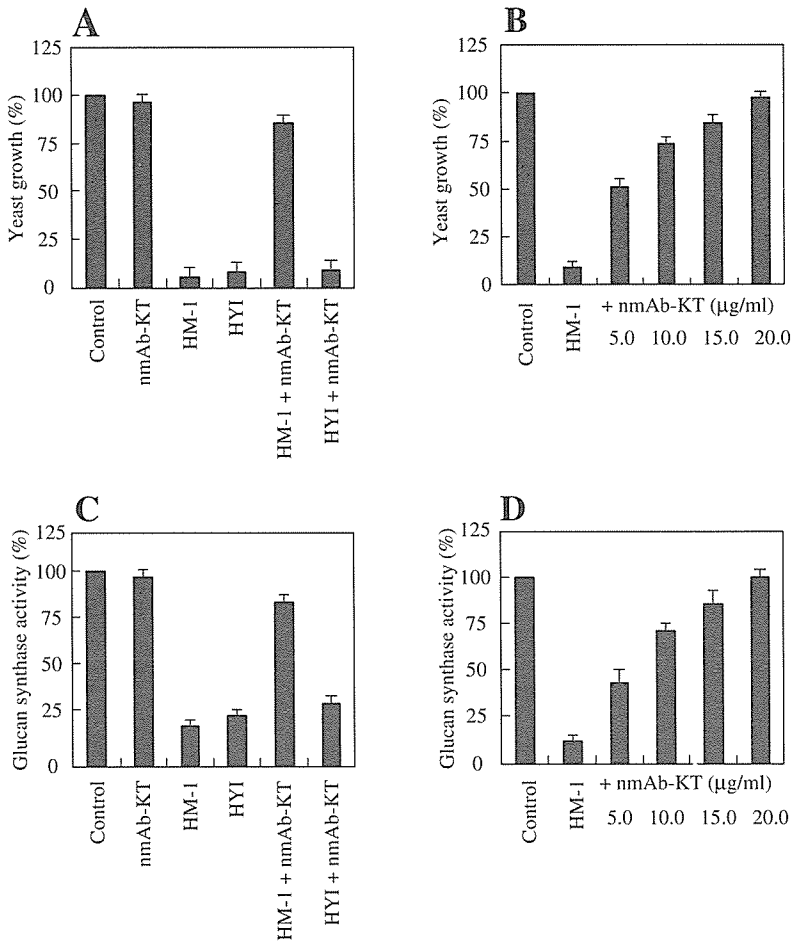

Fig. 1. **Effect of nmAb-KT.** (A) Effect on yeast growth and killing activity of HM-1 and HYI, (B) Dose dependence of the nmAb-KT neutralizing activity on the yeast growth and killing activity of HM-1, (C) Effect on β-1,3-glucan synthase activity and inhibitory activity of HM-1 and HYI. (D) Dose dependence of the nmAb-KT neutralizing activity on the β-1,3-glucan synthase inhibitory activity of HM-1. Assay methods and conditions are described in "MATERIALS AND METHODS." Activity is expressed relative the control sample without nmAb-KT, HM-1 and HYI taken as 100%. Data represent the percentage means of three experiments ± SE.

SPR Analysis of HM-1 and HYI—Real-time measurement of the interaction between nmAb-KT and HM-1 or HYI was done using a BIAcore X biosensor system at 25°C. In the immobilization experiments, HBS-EP buffer [10 mM HEPES, 150 mM NaCl, 3 mM EDTA, 0.005% polysorbate 20 (pH 7.4)] was used as the eluent buffer at a flow rate of 10 μl/min. Immobilization of nmAb-KT on a CM5 sensor chip was achieved by the standard amine coupling method except for the activation. Briefly, 35 μg/ml of nmAb-KT diluted in 10 mM sodium acetate (pH 5.0) was injected into the biosensor surface, which was activated with a 1:1 mixture of 120 μl of 200 mM *N*-ethyl-*N'*-(3-dimethylaminopropyl)carbodiimide hydrochloride and 50 mM *N*-hydroxysuccinimide, and then 120 μl of 1 M ethanolamine (pH 8.5) was injected to inactivate the unreacted reagents. Nearly 3,000 resonance units of nmAb-KT were immobilized. One channel of each sensor chip treated in the same way without nmAb-KT was used as a control for the nonspecific binding of HM-1 or HYI to the carboxymethylated dextran surface. Purified HM-1 and HYI proteins were analyzed at a concentration of 6.25–100 nM. After each measurement, the chip surface was regenerated with 20 μl of 1 mM HCl. HM-1 overlapping peptides and the HYI nanopeptide were analyzed at a concentration of 500 nM. Peptide P6 was analyzed at a concentration of 31.3–500 nM. After each measurement, the chip surface was regenerated with 6 μl of 10 mM HCl. Kinetic sensorgram curves were evaluated with BIAevaluation 3.0 to find the association rate constant, k_{on}, and dissociation rate constant, k_{off}. The dissociation constant, K_d, was calculated from the equation $K_d = k_{off}/k_{on}$.

Peptide Analysis by Growth Inhibition Assay—To determine the effect of overlapping HM-1 peptides and HYI nanopeptide on yeast growth, approximately 4×10^6 cells/ml of *S. cerevisiae* A451 were incubated in YPD medium containing 10 μM of each peptide or 4.21 nM of HM-1 or peptide P6 combined with different concentrations of nmAb-KT at 30°C for 8 h. Yeast growth was measured by the absorbance at 600 nm.

Peptide Binding Analysis by Dot Blotting—ProBlott membranes were placed in a dot blotting apparatus (Biocraft Inc), and the defined areas were coated with 0.1 μg each of the thirteen synthetic overlapping HM-1 peptides or the HYI nanopeptide. The membranes were blocked with 2% non-fat dry milk in TBS for 1 h at room temperature, washed with TBS-T, incubated with nmAb-KT as the primary monoclonal antibody for 2 h at room temperature, and then washed three times with TBS-T. Bound peptides were detected by incubating the membranes with a 1:5,000 dilution of alkaline phosphatase conjugated anti-mouse goat IgG for 1 h at room temperature, followed by staining with Western blue.

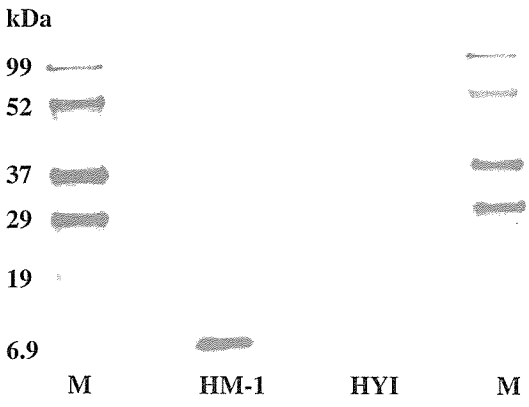

Fig. 2. **Western blot analysis of HM-1 and HYI.** Purified HM-1 and HYI were subjected to electrophoresis, electroblotted and detected using nmAb-KT as the primary antibody as described in "MATERIALS AND METHODS." M: molecular weight standards (lanes 1 and 4), HM-1 (lane 2), and HYI (lane 3).

RESULTS

Characterization of nmAb-KT—nmAb-KT was classified as IgG1(κ) by a mouse monoclonal antibody isotyping kit. Because the typing characterization reveals an antibody structure, its use might be desirable for some applications including immunological techniques. SDS-PAGE showed only heavy and light chain bands with molecular masses of about 57 kDa and 25 kDa, respectively, indicating the purity of the antibody. Adding nmAb-KT to a yeast culture resulted in the yeast retaining 96.4% of growth, but the addition of HM-1 and HYI caused marked inhibition of yeast growth to 5.8% and 8.2% respectively (Fig. 1A). Including nmAb-KT with HM-1 produced an 85% recovery in yeast growth, but including nmAb-KT with HYI produced no recovery (9.0% growth), even at a concentration 15 μg/ml nmAb-KT. Adding nmAb-KT resulted in 97.3% on β-1,3-glucan synthase activity being retained, but HM-1 and HYI reduced β-1,3-glucan synthase activity to 20.8% and 26.0% of control, respectively (Fig. 1C). Including nmAb-KT with HM-1 produced a maximum recovery of β-1,3-glucan synthase activity to 87.3%, but including nmAb-KT with HYI produced a low recovery to 32%, even at a concentration 15 μg/ml nmAb-KT. Our studies show the dose dependence of nmAb-KT on yeast killing activity (Fig. 1B) and β-1,3-glucan synthase inhibitory activity (Fig. 1D). The data also strongly suggest that nmAb-KT can neutralize the killing and inhibitory activities of β-1,3-glucan synthase by HM-1 specifically, and that it does not interfere with either activity of HYI, even though the primary structures of HM-1 and HYI share a high degree of homology (*10*, *11*).

Binding Specificities of nmAb-KT by Western Blot Analysis—Figure 2 shows a clear single band corresponding to the expected molecular mass of about 9,500 Da for HM-1, but HYI did not show a band on the membrane. These results indicate that nmAb-KT binds only to HM-1, and not to HYI. The same result was also obtained by the dot blotting method (data not shown).

SPR Analysis of HM-1 and HYI—The binding specificities and kinetic parameters of purified HM-1 and HYI were determined by SPR analysis. Biacore sensorgrams showed

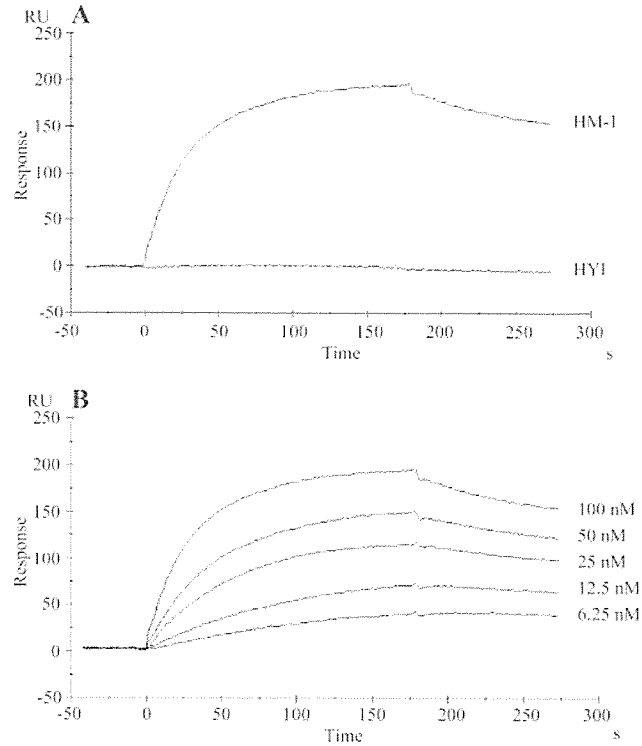

Fig. 3. **SPR analysis of HM-1 and HYI.** Preparation of immobilized nmAb-KT on CM5 sensor chips and the analytical methods are described in "MATERIALS AND METHODS." (A) Association and dissociation of HM-1 and HYI at 100 nM. (B) HM-1 signals at different concentrations in the range of 6.25–100 nM. RU: resonance units.

Table 2. **Kinetic parameters for the binding of nmAb-KT to HM-1 and HYI as measured by SPR analysis.**

Analyte	k_{on} ($\times 10^5$ M^{-1} s^{-1})	k_{off} ($\times 10^{-3}$ s^{-1})	K_d ($\times 10^{-9}$ M)
HM-1	3.3	1.81	5.48
HYI	ND	ND	ND

The kinetic constants for HM-1 and HYI were determined using a BIAcore biosensor: k_{on}, association rate constant; k_{off}, dissociation rate constant; K_d value was calculated as $K_d = k_{off}/k_{on}$. ND, signals not detected.

the degree of interaction between immobilized nmAb-KT and HM-1 or HYI (Fig. 3, A and B). The kinetic data from SPR analysis showed that HM-1 has a strong binding affinity for nmAb-KT, while HYI shows no binding to nmAb-KT. Table 2 shows the calculated values of k_{on}, k_{off} and K_d. The K_d value of HM-1 is 5.48×10^{-9} M. Therefore, we can conclude that nmAb-KT shows strong reactivity toward HM-1, but not toward HYI.

SPR Analysis of HM-1 Peptides—The binding specificities and kinetic parameters of synthetic overlapping HM-1 peptides and the HYI nanopeptide were determined by SPR analysis. Among the thirteen synthetic overlapping HM-1 peptides, P1 is the first (^{1}GDGYLIMCKNCDPN^{14}) and P13 the last (^{78}GFYIRSYRRVE^{88}) in the HM-1 molecule (Table 1). The Biacore sensorgrams showed the degree of interaction between immobilized nmAb-KT and HM-1 peptides or the HYI nanopeptide. Kinetic data from SPR

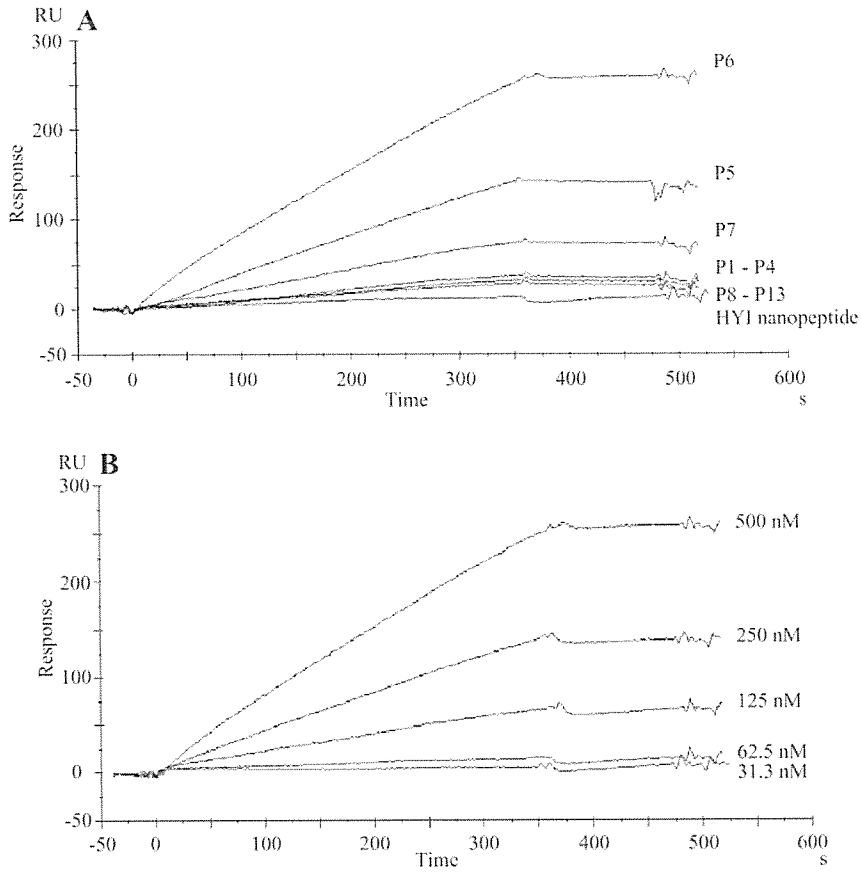

Fig. 4. **SPR analysis of HM-1 overlapping peptides and the HYI nanopeptide.** Preparation of immobilized nmAb-KT on CM5 sensor chips and the analytical methods are described in "MATERIALS AND METHODS." (A) Interaction between nmAb-KT and thirteen HM-1 overlapping peptides or HYI nanopeptide at 500 nM. (B) Peptide P6 signals at different concentrations in the range of 31.3–500 nM.

Table 3. **Kinetic parameters for the binding of nmAb-KT to HM-1 peptide P6 and HYI nanopeptide as measured by SPR analysis.**

Analyte	k_{on} ($\times 10\ M^{-1}\ s^{-1}$)	k_{off} ($\times 10^{-4}\ s^{-1}$)	K_d ($\times 10^{-6}$ M)
HM-1 peptide P6	4.72	6.92	1.47
HYI nanopeptide	ND	ND	ND

The kinetic constants of HM-1 peptide P6 and HYI nanopeptide were determined using a BIAcore biosensor: k_{on}, association rate constant; k_{off}, dissociation rate constant; K_d value was calculated as $K_d = k_{off}/k_{on}$. ND, signals not detected.

analysis showed that HM-1 peptide P6 (^{39}TGGSTDGKQG^{48}) has a marked binding affinity for nmAb-KT and the neighboring peptide P5 (^{33}NVHWMVTGGST^{43}), and that P7 (^{44}DGKQGCATIWEGS^{56}) has a weaker binding affinity for nmAb-KT (Fig. 4A). The HYI nanopeptide, corresponding to the same position in HYI as HM-1 peptide P6 (*11*), showed no signals that indicated binding to nmAb-KT (Fig. 4A). Because of these results, peptide P6 was examined more closely at different concentrations to determine the precise kinetic parameters (Fig. 4B). Table 3 shows the calculated values of k_{on}, k_{off} and K_d. The K_d value of HM-1 peptide P6 is 1.47×10^{-6} M. These results strongly confirm that nmAb-KT recognizes peptide P6 position in HM-1.

Peptide Analysis of nmAb-KT—Peptide analysis of nmAb-KT was performed by yeast growth inhibition assays. All thirteen overlapping peptides and the HYI nanopeptide had little effect on yeast growth, except the P5, P6 and P7 peptides, which showed greater inhibition of yeast growth (Fig. 5A). The killing activity of P6 blocked in a dose-dependent manner by the addition of nmAb-KT (Fig. 5B), indicating that peptide P6 reacts with nmAb-KT. Because the strong inhibitory effect of peptide P6 was reduced by nmAb-KT, P6 could be the specific epitope for nmAb-KT.

Dot Blotting Analysis—To investigate the epitope for nmAb-KT in the HM-1 molecule, the binding specificities of nmAb-KT to thirteen synthetic overlapping HM-1 peptides and the HYI nanopeptide were analyzed by dot blot analysis (Fig. 6). Among thirteen overlapping peptides tested, peptides P5, P6 and P7 showed strong binding to nmAb-KT (Fig. 6A). Figure 6B shows the strongest binding specificities of peptide P6 with nmAb-KT, while the HYI nanopeptide, corresponding to the same position in HYI, showed no binding to nmAb-KT. This result is in good agreement with the SPR analysis, which indicated that the epitope for nmAb-KT is localized within HM-1 at positions 39–48.

DISCUSSION

The identification and characterization of the epitope of an antibody that neutralizes killing activity is inevitably important to understanding the structure and function of the relationship of the killer toxin, and for the use of killer proteins or antibodies in agriculture and the clinical field. Yamamoto *et al.* (*8*) raised an nmAb-KT that can

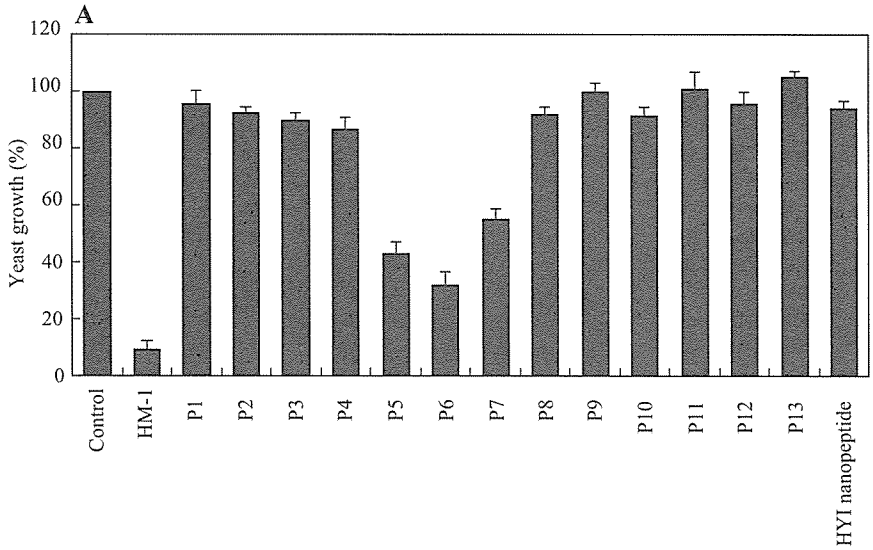

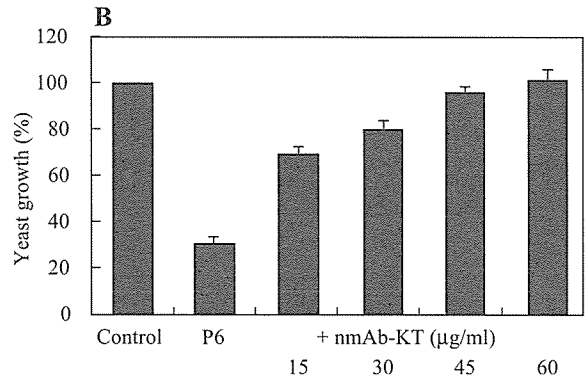

Fig. 5. **Peptide analysis of nmAb-KT.** The growth inhibition assays and assays of the killing activity of HM-1 overlapping peptides are described in "MATERIALS AND METHODS." (A) Effect of HM-1 peptides and the HYI nanopeptide on *S. cerevisiae* A451 growth. (B) Dose dependence of neutralizing effect of nmAb-KT on the killing activity of P6. Activity is expressed relative to the control sample without peptide and nmAb-KT taken as 100%. Data represent the percentage means of three experiments ± SE.

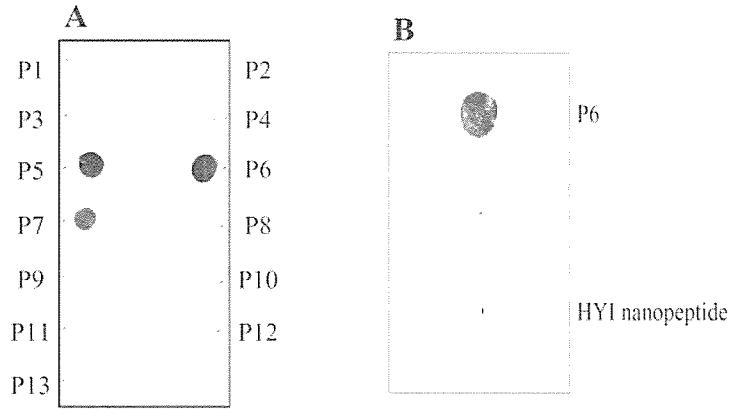

Fig. 6. **Peptide binding assay by dot blotting analysis.** Dot blotting and detection using nmAb-KT as a primary antibody are described in "MATERIALS AND METHODS." (A) Thirteen overlapping peptides adsorbed on the membrane. (B) HM-1 peptide P6 and HYI nanopeptide adsorbed on membrane.

neutralize the killing activity of HM-1. Killer toxins by themselves have been proposed as potential fungistatic agents (*17*, *18*). However, the protein and immunogenic nature of killer toxins have hampered their direct application to eradicating systemic infections of pathogenic fungi. Whether the anti-fungal activity of a given killer toxin is strong enough to control the growth of pathogenic organisms effectively is not clear, and whether injected killer toxins have anti-fungal efficacy over a long period against immune responses is also doubtful. Recently, using recombinant DNA technology and a phage display system, we applied nmAb-KT for idiotypic vaccination to produce anti-idiotypic antibodies that mimic the internal image of HM-1 (manuscript submitted). We were successful in obtaining single-chain fragment variable anti-idiotypic antibodies that showed strong fungicidal activity against various clinically important pathogens. Our preliminary studies also showed that another killer toxin, HYI, despite its

close similarity to HM-1 in structure and glucan synthase inhibitory activity, is not neutralized by nmAb-KT. Our results prompted us to characterize the active site of HM-1 responsible for the expression of the killing activity and the epitope site bound by nmAb-KT.

In this study we generated a new sandwich ELISA method using nmAb-KT, so that small amounts of HM-1 could be quantitated more precisely (data not shown). We then characterized the epitope of HM-1 recognized by nmAb-KT that neutralizes the killing and glucan synthase inhibitory activity of HM-1 (Fig. 1, A and C). The nmAb-KT neutralization effect on yeast killing and glucan synthase inhibitory activity by HM-1 were analyzed precisely by observing the dose dependence of nmAb-KT, and these results confirmed that nmAb-KT strictly binds and neutralizes the killing and inhibitory activities of HM-1 (Fig. 1, B and D). Scanning analysis of synthetic overlapping HM-1 peptides by growth inhibition assays showed that peptide P6 and its neighboring peptides have marked killing activity on yeast growth (Fig. 5A). The nmAb-KT neutralization effects on yeast killing activity by P6 were analyzed precisely by observing the dose dependence of nmAb-KT, and these results indicated that nmAb-KT binds and neutralizes the killing activity of P6 (Fig. 5B). These combined observations strongly confirm that the nmAb-KT epitope lies within HM-1 peptide P6 (^{39}TGGSTDGKQG^{48}), which could be part of the active site of the HM-1 killer function. Consistently, HYI, which is not neutralized by nmAb-KT, contains a dissimilar amino acid sequence ^{39}TGESNGQQG^{47} in the corresponding region, and shows only about 50% local homology to HM-1. Noteworthy is that HYI differs from HM-1 only in the ^{39}TGESNGQQG^{47} region, despite its overall homology being as high as 87%. SPR analysis showed that nmAb-KT binds HM-1 with a high affinity ($K_d = 5.48 \times 10^{-9}$ M), but does not bind to HYI (Fig. 3, A and B; Table 2).

In addition to this study, we tried spot analysis, in which synthetic peptides are covalently linked to a membrane filter using an oligopeptide spacer (*19*), to find the epitope recognized by nmAb-KT. We synthesized and analyzed 39 peptides comprising 12 amino acid residues with 10 residues overlapping the next peptide and linked to the membrane by two β-alanine spacers (*14*), but we detected no positive spot with nmAb-KT. The most probable explanation is that steric hindrance caused by the covalent linkage of the peptides to the membrane filter may prevent the binding of large molecules such as nmAb-KT.

In this study, we used soluble peptides to identify the epitope position on HM-1 for nmAb-KT. From the binding ability of nmAb-KT and the homology between HM-1 and HYI, we propose the nmAb-KT epitope to be as follows. In addition to P6, overlapping peptides P5 and P7 bound strongly to nmAb-KT. Amino acids ^{39}TG^{40} and ^{47}QG^{48} in P6 are homologous, respectively, to ^{39}TG^{40} and ^{46}QG^{47} in the HYI nanopeptide (Table 1). Therefore, considering that a general protein epitope consists of 5 - 6 amino acid residues, we propose the epitope for nmAb-KT to be at the position ^{41}GSTDGK^{46} in HM-1. Also, molecular modeling of HM-1 using RasMol software (Fig. 7) showed sequence 41–46 protruding from the surface of the HM-1 molecule (*9*), and residues, G-41, T-43, D-44 and K-46 in ^{41}GSTDGK^{46} are different from the corresponding residue in HYI.

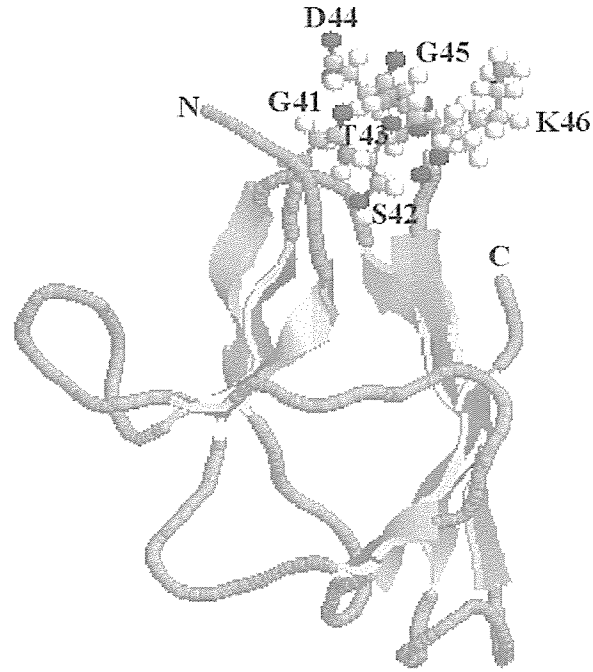

Fig. 7. **Three-dimensional structure of HM-1**. Image showing the three-dimensional structure of HM-1 drawn using RasMol software. The binding epitope for nmAb-KT in positions 41–46 is shown as balls and sticks. N and C indicate the N-terminus and C-terminus of HM-1, respectively.

Peptide binding assays showed that nmAb-KT reacts most strongly with HM-1 overlapping peptide P6, but not with the HYI nanopeptide (Fig. 6, A and B). Peptide and nmAb-KT binding analyses carried out by SPR analysis showed that HM-1 peptide P6 binds to nmAb-KT with a calculated $K_d = 1.47 \times 10^{-6}$ M, but that the HYI nanopeptide showed no signals for nmAb-KT (Fig. 4, A and B; Table 3). These results suggest that HM-1 overlapping peptide P6 is an active site for the expression of the killing activity of HM-1. The amino acid sequence of the epitope for nmAb-KT evaluated in this study agrees well with our previous study (*20*), which showed D-44 and K-46 as essential amino acids for the killing activity of HM-1. The absence of D-44 and K-46, in addition to G-41 and T-43, in the HYI sequence can be assumed to be the most probable reason for why HYI does not bind to nmAb-KT.

The variety of techniques used in this study provide a better understanding of both the binding and neutralizing activity of nmAb-KT for HM-1 and HYI. The experimental results obtained and described in this study are useful for determining the epitope for nmAb-KT and can be used as potential tools for further investigations of this antibody as related to its possible clinical applications.

This work was supported by a grant from the Ministry of Education, Science, Sports and Culture of Japan.

REFERENCES

1. Starmer, W.T., Ganter, P.F., Aberdeen, V., Lachance, M.A., and Phaff, H.J. (1987) The ecological role of killer yeasts in natural communities of yeasts. *Can. J. Microbiol.* **33**, 783–796

2. Nomoto, H., Kitano, K., Shimazaki, T., Kodama, K., and Hara, S. (1984) Distribution of killer yeasts in the genus *Hansenula*. *Agric. Biol. Chem.* **48**, 807–809
3. Kimura, T., Kitamoto, N., Ohta, Y., Kito, Y., and Iimura, Y.J. (1995) Structural relationships among killer toxins secreted from the killer strains of the genus *Williopsis* .*J. Ferment. Bioeng.* **80**, 85–87
4. Young, T.W. and Yagiu, M. (1978) A comparison of the killer character in different yeasts and its classification. *Antonie Van Leeuwenhoek* **44**, 59–77
5. Ashida, S., Shimazaki, T., Kitano, K., and Hara, S. (1983) New killer toxin of *Hansenula mrakii*. *Agric. Biol. Chem.* **47**, 2953–2955
6. Ohta, Y., Tsukada, Y., and Sugimori, T. (1984) Production, purification and characterization of HYI, an anti-yeast substance, produced by *Hansenula saturnus*. *Agric. Biol. Chem.* **48**, 903–908
7. Yamamoto, T., Hiratani, T., Hirata, H., Imai, M., and Yamaguchi, H. (1986) Killer toxin from *Hansenula mrakii* selectively inhibits cell wall synthesis in a sensitive yeast. *FEBS Lett.* **197**, 50–59
8. Yamamoto, T., Imai, M., Tachibana, K., and Mayumi, M. (1986) Application of monoclonal antibodies to the isolation and characterization of a killer toxin secreted by *Hansenula mrakii*. *FEBS Lett.* **195**, 253–257
9. Anutch, W., Guntert, P., and Wuthrich, K. (1996) Ancestral beta gamma-crystallin precursor structure in a yeast killer toxin. *Nat. Struct. Biol.* **3**, 662–665
10. Kimura, T., Kitamoto, N., Matsuoka, K., Nakamura, K., Iimura, Y., and Kito, Y. (1993) Isolation and nucleotide sequences of the genes encoding killer toxins from *Hansenula mrakii* and *H. saturnus*. *Gene* **137**, 265–270
11. Komiyama, T., Ohta, T., Furuichi, Y., Ohta, Y., and Tsukada, Y. (1995) Structure and activity of HYI killer toxin from *Hansenula saturnus*. *Biol. Pharm. Bull.* **18**, 1057–1059
12. Komiyama, T., Shirai, T., Ohta, T., Urakami, H., Furuichi, Y., Ohta, Y., and Tsukada, Y. (1998) Action properties of HYI killer toxin from *Williopsis saturnus* var. *saturnus*, and antibiotics, aculeacin A and papulacandin B. *Biol. Pharm. Bull.* **21**, 1013–1019
13. Komiyama, T., Ohta, T., Urakami, H., Shiratori, Y., Takasuka, T., Satoh, M., Watanabe, T., and Furuichi, Y. (1996) Pore formation on proliferating yeast *Saccharomyces cerevisiae* cell buds by HM-1 killer toxin. *J. Biochem.* **119**, 731–736
14. Komiyama, T., Zhang, Q.Z., Miyamoto, M., Selvakumar, D., and Furuichi, Y. (2004) Monoclonal antibodies and sandwich ELISA for quantitation of HM-1 killer toxin. *Biol. Pharm. Bull.* **27**, 691–693
15. Kasahara, S., Yamada, H., Mio, T., Shiratori, Y., Miyamoto, C., Yabe, T., Nakajima, T., Ichishima, E., and Furuichi, Y. (1994) Cloning of the *Saccharomyces cerevisiae* gene whose overexpression overcomes the effects of HM-1 killer toxin, which inhibits beta-glucan synthesis. *J. Bacteriol.* **176**, 1488–1499
16. Cabib, E. and Kang, M.S. (1987) Fungal 1,3-β-glucan synthase in *Methods in Enzymology* (Ginsberg, V., ed.) **138**, 637–642, Academic press, New York
17. Yamamoto, T., Uchida, K., and Hiratani, T. (1988) In vitro activity of the killer toxin from yeast *Hansenula mrakii* against yeasts and molds. *J Antibiot.* **XLI**, 398–403
18. Polonelli, L., Lorenzini, R., Bernardis, D.F., and Morace, G. (1986) Potential therapeutic effect of yeast killer toxin. *Mycopathologia* **96**, 103–107
19. Frank, R. (1992) Spot-synthesis: An easy technique for the positionally addressable, parallel chemical synthesis on a membrane support. *Tetrahedron* **48**, 9217–9232
20. Miyamoto, M., Han, G.D., Kimura, T., Furuichi, Y., and Komiyama, T. (2005) Alanine-scanning mutagenesis of HM-1 killer toxin and the essential residues for killing activity. *J. Biochem.* **137**, 517–522

Published online 8 September 2006

Nucleic Acids Research, 2006, Vol. 34, No. 17 ***4711–4721***
doi:10.1093/nar/gkl663

Exportin-5 orthologues are functionally divergent among species

Satoshi Shibata[1], Mitsuho Sasaki[1], Takashi Miki[1], Akira Shimamoto[3], Yasuhiro Furuichi[3], Jun Katahira[1,2,*] and Yoshihiro Yoneda[1,2,*]

[1]Department of Cell Biology and Neuroscience, Graduate School of Medicine and [2]Biomolecular Networks Laboratories, Biomolecular Dynamics Group, Graduate School of Frontier Biosciences, Osaka University, 1-3 Yamadaoka, Suita, Osaka 565-0871, Japan and [3]Department of Target Discovery, GeneCare Research Institute, 200 Kajiwara, Kamakura, Kanagawa 247-0063, Japan

Received July 4, 2006; Revised August 14, 2006; Accepted August 24, 2006

ABSTRACT

Exportin-5, an evolutionarily conserved nuclear export factor belonging to the importin-β family of proteins, is known to play a role in the nuclear export of small noncoding RNAs such as precursors of microRNA, viral minihelix RNA and a subset of tRNAs in mammalian cells. In this study, we show that the exportin-5 orthologues from different species such as human, fruit fly and yeast exhibit diverged functions. We found that Msn5p, a yeast exportin-5 orthologue, binds double-stranded RNAs and that it prefers a shorter 22 nt, double-stranded RNA to ~80 nt pre-miRNA, even though both of these RNAs share a similar terminal structure. Furthermore, we found that *Drosophila* exportin-5 binds pre-miRNAs and that amongst the exportin-5 orthologues tested, it shows the highest affinity for tRNAs. The knockdown of *Drosophila* exportin-5 in cultured cells decreased the amounts of tRNA as well as miRNA, whereas the knock down of human exportin-5 in cultured cells affected only miRNA but not tRNA levels. These results indicate that double-stranded RNA binding ability is an inherited functional characteristic of the exportin-5 orthologues and that *Drosophila* exportin-5 functions as an exporter of tRNAs as well as pre-miRNAs in the fruit fly that lacks the orthologous gene for exportin-t.

INTRODUCTION

Since the nucleus and the cytoplasm are physically separated compartments in eukaryotic cells, different classes of RNAs and proteins are transported into and out of the nucleus via the nuclear pore complex. Shuttling transporters are indispensable for the signal mediated nulceo-cytoplasmic transport of different cargoes. The importin-β family proteins comprise one major class of nucleo-cytoplasmic transporters (1–4). The importin-β family proteins are subdivided into two major classes, based on their directionality of transport i.e.; importins function in the nuclear import, whereas exportins are engaged in the nuclear export of various cargoes. The small nuclear GTPase Ran plays a pivotal role, in dictating the directionality of transport mediated by the importin-β family proteins (5,6).

Exportin-5 (Exp5) has been identified as an exportin for various RNAs including viral mini-helix RNA and precursors of microRNA (pre-miRNAs) (7–11). These non-coding RNAs share common structural characteristics, such as a small size, hairpin-like fold-back structures due to intramolecular base pairing, and a 2–3 nt protrusion at their 3′ ends, which are also known as common structural features of RNase III-processed RNAs. Indeed, a recent report demonstrated that human (hs) Exp5 recognizes pre-microRNAs through their double-stranded (ds) stem and the short overhang at the 3′-end that are produced by nuclear RNaseIII Drosha cleavage (12).

Msn5p, the budding yeast orthologue of mammalian Exp5, was originally identified as an exportin for a subset of proteins, not all but most of which are phosphorylated (13–18). Since there is no sequence similarity among these protein cargoes, proteinaceous nuclear export signal (NES) specific for Msn5p is still elusive. In addition to these cargoes, Msn5p may also function as an exportin for tRNAs, albeit it was only indirectly shown (19). The exportin that was first assigned as being specific for tRNAs is Los1p in yeast and exportin-t (Exp-t) in mammals (20–24). Although yeast strains lacking either *LOS1* or *MSN5* alone revealed only moderate defects in the nuclear export of tRNAs (24–26), the double knockout strain, lacking both of these genes,

*To whom correspondence should be addressed. Tel: +81 6 6879 4605; Fax: +81 6 6879 4609; Email: yyoneda@anat3.med.osaka-u.ac.jp
*Correspondence may also be addressed to Jun Katahira. Tel: +81 6 6879 4606; Fax: +81 6 6879 4609; Email: katahira@anat3.med.osaka-u.ac.jp
Present address:
Akira Shimamoto, Department of Cellular and Molecular Biology, Division of Integrated Medical Science, Program for Biomedical Research, Graduate School of Biomedical Sciences, Hiroshima University, 1-2-3 Kasumi, Minami-ku, Hiroshima 734-8553, Japan

showed a significant defect in the nuclear export of tRNAs (19). Using a *Xenopus* oocyte microinjection system, it was shown that both Exp-t and Exp5 of mammalian origin also promoted the nuclear export of tRNAs, although the potency of Exp-t was higher than that of Exp5 (27).

HsExp-t binds to the TψC and acceptor arms of tRNA under *in vitro* conditions (20). Both Bohnsack *et al.* and Calado *et al.* have suggested that the mechanism of recognition of tRNAs by Exp5 are different from that by Exp-t, based on their observations that Exp5, but not Exp-t, is able to form a ternary complex with tRNA along with a tRNA binding protein, eEF1A (27,28). In plant *Arabidopsis*, a defect in tRNA processing was observed in an Exp-t orthologue PAUSED (PSD) mutant, but not in an Exp5 orthologue HASTY (HST) mutant (29–32). As mentioned above, mammalian Exp5 facilitates the nuclear export of pre-miRNA and the viral mini helix RNA (7–9), but other cargoes for Exp-t, except for tRNAs have not yet been identified. These cumulative findings suggest that in most organisms, including animals and plants, Exp5 orthologues may play major roles in pre-miRNA export, whereas it comprises a minor export route for tRNAs.

Interestingly, however, it was predicted that no Exp-t orthologous gene exists in several arthropods including *Drosophila melanogaster* (dm) (33). To date, the issue of how tRNA export is achieved in such organisms remains unknown. In this study, we compared the functional characteristics of three Exp5 orthologues from different species to determine whether Exp5 orthologues from different organisms function in different manners. Although we found that all the Exp5 orthologues examined were able to bind both pre-miRNAs and tRNAs, there are significant differences in their substrate preferences. Yeast Msn5p exhibited a higher affinity for a short 22 bp dsRNA than to a ~80 bp pre-miRNA with the hairpin-like fold-back structure. Though hsExp5 was able to recognize tRNAs as cargoes, the binding of hsExp5 to pre-miRNA was not inhibited by an excess amount of tRNA. In contrast, we found that tRNAs efficiently inhibited the interaction between dmExp5 and pre-miRNA. The RNAi-induced knockdown of the expression of dmExp5 in *Drosophila* Schneider's 2 cells caused a decrease in the expression of both tRNA and miRNA. The down regulation of hsExp5 in human cells, on the other hand, resulted in a decrease in miRNA but not tRNA. These results indicate that, in *Drosophila* cells, dmExp5 plays a central role in the nuclear export of tRNA and miRNA and that dsRNA binding ability is an inherited functional property of the Exp5 orthologues. The latter indication suggests the intriguing possibility that dsRNA may be widely involved in the nuclear export of protein cargoes by yeast Msn5p.

MATERIALS AND METHODS

Plasmid construction

To construct a template for pT7-pre-miR-30, two oligonucleotides 5′- GATCCTTTCTAATACGACTCACTATAGGGGCGACTGTAAACATCCTCGACTGGAAGCTGTGAAGCCACAGATGGGCTTTCAGTCGGATGTTTGCAGCTGCTGCATG -3′ and 5′-CAGCAGCTGCAAACATCCGACTGAAAGCCCATCTGTGGCTTCACAGCTTCCAGTCGAGGATGTTTACAGTCGCCCCTATAGTGAGTCGTATTAGAAAG-3′ (underline indicates the T7 promoter sequence) were annealed and ligated to the pUC18 vector that had been treated with BamHI and SphI. The template plasmids encoding U1ΔSm and tRNA-Met were generous gifts from M. Ohno, Kyoto University.

The cDNAs for hsExp5 and dmExp5 (GenBank accession numbers, hsExp5: AF298880, dmExp5: AF222746.1) were amplified by RT–PCR, subcloned into the NotI–XhoI site of the pcDNA3 vector (Invitrogen) together with an oligonucleotide linker encoding a FLAG peptide tag (DYKDDDDK) and is referred to as pcDNA/hsExp5 and pcDNA/dmExp5, respectively. For the construction of an *Escherichia coli* expression vector, the cDNA of hsExp5 was amplified by PCR and cloned into the pQE60 vector (Qiagen) that had been linearized by NcoI–BglII double digestion. The cDNA for Msn5p (GenBank accession number: X93302) was amplified by PCR using pTYE292 (a gift from T. Yoshihisa, Nagoya University) as a template and cloned into the NcoI–BamHI site of the pQE60 vector. The cDNA of dmExp5 was amplified by PCR and cloned into the BamHI–XhoI site of the pET21a (+) vector (Stratagene). DNA fragments encoding human exportin-1 were amplified by PCR using pB-hCRM1 (34) and cloned into pQE60 vector and pGEX-6P vector (GE Healthcare). The cDNA of *Drosophila* Ran (GenBank accession number: AF233584) was amplified by RT–PCR and cloned into pBluescript SK (+) vector (Stratagene). To generate the dmRanQ69L mutant, this plasmid was mutated using a QuikChange site-directed mutagenesis kit (Stratagene) using the following primers: the forward primer, 5′-TGGGATACCGCTGGCCTGGAGAAGTTCGGCGGGCTGCGCG-3′ and the reverse primer, 5′-CCCGCCGAACTTCTCCAGGCCAGCGGTATCCCACACATTG-3′. The mutated DNA fragment was cloned into the pGEX-6p vector. A DNA fragment encoding Gsp1pQ71L was amplified by PCR using pTYE297 as a template (a gift from T. Yoshihisa) and cloned into the pGEX-6p vector. Construction of the *E.coli* expression vectors for human RanQ69L has been described elsewhere (35). The pQE60-Exp-t vector (20) was a gift from M. Ohno. To obtain an expression vector for hsExp5 in S2 cells, pcDNA/hsExp5 was digested at the NotI–XhoI site and the resulting DNA fragment encoding FLAG-hsExp5 was ligated to the pMT/V5 His A vector (Invitrogen) that had been treated with NotI and XhoI.

For preparation of dsRNAs encoding dmDrosha (GenBank accession number: AF116572) and dmDGCR8 (GenBank accession number: NM_143622), the full-length cDNAs of dmDrosha and dmDGCR8 were cloned by RT–PCR and ligated into the EcoRV site of the pBluescript SK (+) vector by blunt-end ligation.

Cell culture and establishment of stable cell lines

Drosophila Schneider's 2 (S2) cells were cultured in complete Schneider's *Drosophila* medium (Invitrogen) containing 10% heat-inactivated fetal bovine serum (FBS) at 28°C. S2 cells (3×10^6) in 3 ml of complete Schneider's *Drosophila* medium were seeded in 35 mm dishes and grown for 12–16 h

prior to transfection. The pMT/V5-His vectors, which express nothing (empty) or hsExp5, were co-transfected with pCoHygro (Invitrogen) using the calcium phosphate transfection procedure. Four days after transfection, stable cells were selected by culturing them in complete medium containing 300 μg/ml Hygromicin-B (Wako) for more than 3 weeks. After examining the stable expression of hsExp5 by western blot using an anti-penta-His antibody, the cells were cultured in the same medium containing 300 μg/ml Hygromycin-B (Wako).

293F cells were cultured in DMEM (Sigma) containing 10% FBS at 37°C in 5% CO_2 atmosphere.

Antibodies

Mice were immunized against residues 712–1214 of hsExp5, which was expressed as a His-tagged protein in *E.coli*. A pool of the sera, the specificities of which were individually confirmed by western blot using a total cell extract of 293F cells (data not shown), was used as a polyclonal anti-hsExp5 antibody. Mouse monoclonal anti-GAPDH, anti-FLAG M2 and anti-penta-His antibodies were purchased from Ambion, Sigma and Qiagen, respectively.

Recombinant proteins

A series of exportins used in electrophoresis mobility sift assays were synthesized *in vitro* using pcDNA/hsExp5 or pcDNA/dmExp5 as template. *In vitro* translation reactions were performed using a rabbit reticulocyte lysate system (Promega) according to the manufacturer's protocol.

The recombinant constitutive active mutants of Ran orthologues were expressed in *E.coli* BL21 and purified as described previously (35).

Histidine-tagged hsExp5 and dmExp5 were expressed in *E.coli* M15 (pREP4) and Rosseta cells, respectively, at 20°C. Msn5p was expressed in *E.coli* M15 (pREP4) at 20°C in 2× YT medium containing 1% glucose. After inducing protein expression, the cells were suspended in a buffer (50 mM Tris–HCl pH 7.5, 700 mM NaCl, 10 mM $MgCl_2$, 5% glycerol, 5 mM β-mercaptoethanol, 10 mM imidazol) and disrupted by sonication. The Exp5 orthologues were purified from soluble supernatants by chromatography on Ni-NTA agarose (Qiagen) followed by a MonoQ (GE Healthcare) FPLC column. The purified Exp5 orthologues were equilibrated with injection buffer (20 mM HEPES–KOH pH 7.5, 110 mM potassium acetate, 2 mM magnesium acetate, 10 mM NaCl) by passing through PD-10 gel filtration columns (GE Healthcare). Histidine-tagged hsExp-t was expressed in *E.coli* XL1 Blue at 37°C in LB medium. The cells were disrupted by sonication and purified by Ni-NTA agarose column chromatography. Histidine-tagged Exp1 was obtained using the same procedure except that the expression was induced at 20°C. CAS and Exp1 were expressed as glutathione *S*-transferase (GST)-tagged fusion proteins and purified by glutathione Sepharose column chromatography according to the manufacture's protocol. The GST moieties of the fusion proteins were removed by PreScission protease (GE healthcare) digestion. These proteins were equilibrated with the injection buffer as described above.

Electrophoresis mobility shift assay

The radio-labeled pre-miR-30 RNA probe (10 000 c.p.m.) and 4.5 μl of reticulocyte lysate (TNT Quick Coupled Transcription/translation systems, Promega) containing *in vitro* translated hsExp5 or dmExp5 were mixed and incubated in the presence or absence of 2 μM constitutive active mutants of Ran orthologues from cognate species. The binding reactions (final volume of 10 μl) were performed in binding buffer (20 mM HEPES–KOH pH 8.0, 150 mM NaCl, 1 mM $MgCl_2$, 10% glycerol, 0.5 mM dithiothreitol,) containing 2 units of RNasin (Promega). For competition assays, 70 nM (for hsExp5 and dmExp5) or 210 nM (for Msn5p) of the recombinant exportins were incubated in binding buffer containing 2 μM of each Ran mutant in a final volume of 10 μl. After incubation for 10 min at room temperature, 2 μl of Blue/Orange 6× loading dye (Promega) was added to these reaction mixtures and the mixture was then applied to 6% non-denaturing polyacrylamide gels. Electrophoresis was carried out at a constant voltage of 10 V/cm at room temperature in 0.5× TBE buffer. RNA–protein complexes were visualized by autoradiography.

In Figure 3C, a RNA-containing fraction was prepared by treating the reticulocyte lysate with proteinase K (Nakalai) followed by phenol/chloroform extraction and ethanol precipitation.

Purified baker's yeast tRNA-phe was purchased from Sigma. For generation of a dsRNA having a 3′ or 5′ overhanging at one end, two RNA oligonucleotides 5′-GGGCUUUCAGUCGGAUGUUUGCAGC-3′ or 5′-GGGCUUUCAGUCGGAUGUUUG-3′ and 5′- UGCAAACAUCCGACUGAAAGC-3′ were mixed in annealing buffer (100 mM potassium acetate, 30 mM HEPES–KOH pH 7.4, 2 mM magnesium acetate), denatured at 90°C for 1 min and annealed by incubating at 37°C for 3 h. The same procedure was used to generate a dsDNA encoding the same sequence as dsRNA. All the oligonucleotides were synthesized in JBIOS Co. Ltd.

The unlabeled pre-miR-30 competitor RNA was generated by the RiboMAX Large Scale RNA Production System-T7 (Promega) according to the manufacture's protocol. The *in vitro* transcribed dsRNAs were purified, quantified by A_{260} nm/A_{280} readings and their integrity was verified by electrophoresis on denaturing polyacrylamide gels.

Immunoprecipitation from rabbit reticulocyte lysate

The anti-penta-His antibody (3.25 μg) immobilized on Protein-G Sepharose beads (GE Healthcare) was preincubated with a mixture of 55 μl of reticulocyte lysate (TNT Quick Coupled Transcription/translation system, Promega) and 0.2 μM of each recombinant exportin in the presence or absence of 1.8 μM of the Ran mutant for 30 min at 4°C. After 3 h at 4°C, the beads were washed three times with binding buffer [50 mM Tris–HCl pH 7.5, 1 mM $Mg(AcO)_2$, 100 mM KOAc]. For the detection of bound proteins by western blot using the anti-penta-His antibody, the bound proteins were eluted by boiling the beads (7% of total) in SDS sample buffer. The remaining sample was treated with proteinase K for 30 min at 50°C, followed by phenol/chloroform extraction and ethanol precipitation to isolate the co-precipitated RNAs.

The RNAs were separated on 6% denaturing polyacrylamide gels and detected by ethidium bromide staining.

RNAi experiments

Preparation of dsRNAs. Templates for GFP, dmExp5, DGCR8 and dmDrosha dsRNAs were amplified by PCR using following primers, GFP/dsRNA: sense primer nt 1–24 and anti-sense primer nt 677–700 of GFP cDNA; dmExp5/dsRNA: sense primer nt 1–24 and anti-sense primer nt 677–700 of dmExp5 cDNA; DGCR8/dsRNA: sense primer nt 1–22 and anti-sense primer nt 700–721 of dmDGCR8 cDNA; Drosha/dsRNA: sense primer nt 1–23 and anti-sense primer nt 680–703 of dmDrosha. These primers contain the T7-promoter sequence (GAATTAATACGACTCACTATAGGG) at their 5′ ends. The PCR products were purified using a QIAEX II Gel Extraction Kit (Qiagen) and then subjected to a RiboMAX Large Scale RNA Production System-T7. The resulting dsRNAs were ethanol-precipitated, redissolved in annealing buffer. Annealing was accomplished by incubating the RNAs at 65°C for 30 min followed by slow cooling to room temperature. The integrity of each dsRNA was verified by electrophoresis on agarose gels followed by ethidium bromide staining.

Preparation of short interfering RNAs

A short interfering RNA (siRNA) to deplete hsExp5 (siExp5) was prepared as described previously (8). Both the sense [5′-UGUGAGGAGGCAUGCUUGUd(TT)-3′] and anti-sense [5′-ACAAGCAUGCCUCCUCACAd(TT)-3′] RNAs were obtained from Takara. An siRNA against DsRed [sense, 5′-CACCGUGAAGCUGAAGGUGd(TT)-3′ and anti-sense, 5′-CACCUUCAGCUUCACGGUGd(TT)-3′] was obtained from Darmacon.

Knockdown in Drosophila S2 cells

Treatment of S2 cells with dsRNA was performed as described previously (36). Briefly, S2 cells were suspended in serum-free Schneider's *Drosophila* medium at a density of 1×10^6 cells/ml. Aliquots of the cell suspension (1 ml) were seeded on six-well culture plates and a final concentration of 74 or 111 nM of each dsRNA was then added. After incubation for 6 h at 28°C, 2 ml of serum-containing Schneider's *Drosophila* medium was added and the cells were further incubated for 3 or 4 days prior to analysis. For the 6 day incubation protocol, an additional dsRNA treatment was performed as above at 3 days after the initial treatment. For complementation studies in S2/hsExp5 cells, the expression of hsExp5 was induced by the addition of $CuSO_4$ to the medium at a final concentration of 500 μM after treatment of the cells with dsRNAs for 24 h. After incubation, the cells were harvested and subjected to total RNA extraction with the TRIzol reagent (Invitrogen) or total protein extraction by boiling in SDS–PAGE sample buffer.

Knockdown in 293F cells

293F cells in six-well culture plates at ~40% confluecy were transfected with siExp5 or siDsRed at a final concentration of 30 μM by Lipofectamine2000 (Invitrogen). At 24 h after the initial siRNA treatment, the second transfection was performed by the same procedure. At 72 h after the initial transfection, the cells were harvested. Total RNA and protein samples were isolated as above.

Northern blot and RT–PCR analysis

For the northern blot, 10 μg of total RNAs were applied to 15% denaturing polyacrylamide gels, electrophoresed and transferred to Hybond-N+ membranes (GE Healthcare). Hybridization was performed for 2 h at 46°C using the PerfectHyb Hybridization Solution (TOYOBO). The following radio-labeled oligonucleotide probes were used. Human let-7a: 5′-AACTATACAACCTACTACCTCA-3′; tRNA-Met: 5′-CAGCACGCTTCCGCTGCGCCACTCT-3′; tRNA-Ser: 5′-ATCGCCTTAACCACTCGGCCACG-3′; fly miR-2: 5′-GCTCCTCAAAGCTGGCTGTGATA-3′; U6 snRNA: 5′-GGCCATGCTAATCTTCTCTGTA-3′; and fly U1 snRNA: 5′-GTTAACCTCTACGCCAGGTAAGT-3′. For RT–PCR analysis, the first strand cDNAs were synthesized with SuperScript III Reverse Transcriptase (Invitrogen) using oligo(dT)20 primer according to manufacture's instruction. PCR were carried out using *Taq* DNA polymerase and the following primer sets were used. For dmExp5: forward primer, 5′-AATGGACGAGAACAAGGCCG-3′, and reverse primer, 5′-CACTTCTCCGGCCCAAAGAG-3′; for GAPDH: forward primer, 5′-CAGAAGACCGTCGACGGTCC-3′, and reverse primer, 5′-AGTCCTTGCTCTGCATATAC-3′; for dmDrosha: forward primer, 5′-GCCGAAATATGCCGTGTATG-3′, and reverse primer, 5′-TCATCCCAGCGAAGATTTTGAAG-3′; for dmDGCR8: forward primer, 5′-AAAACGCAGCCACGCCTTAC-3′, and reverse primer, 5′-TCAAAGTTCCACGTTGTTCAAA-3′. The PCR products were electrophoresed in 1% agarose gels and visualized by ethidium bromide staining. Contamination of genomic DNA was checked by performing RT–PCR without reverse transcription step (data not shown).

RESULTS

Double-stranded RNA binding abilities are conserved features of the Exp5 orthologues

Although it has been recently demonstrated that hsExp5 functions as an exportin for pre-miRNAs and is able to bind them *in vitro*, the issue of whether the abilities of Exp5 orthologues to recognize the RNA cargoes are evolutionarily conserved remains unknown. Therefore, the binding of bacterially expressed hsExp5, dmExp5 and Msn5p (Figure 1A) to pre-miRNA was first examined by an electrophoresis mobility shift assay (EMSA), in which *in vitro* transcribed radio-labeled human pre-miR-30 was used as a probe. The labeled pre-miR-30 probe was efficiently exported from *Xenopus* oocyte nuclei (data not shown), indicating that this probe is functional. Since exportins require Ran-GTP for forming a stable complex with their cargoes, purified RanQ69L-GTP and its orthologous mutants from cognate species, which are deficient in GTP hydrolysis, were added exogenously. We observed that hsExp5 and dmExp5 efficiently bound pre-miR-30 (Figure 1B, hsExp5: lanes 1–5; dmExp5: lanes 6–10), whereas Msn5p exhibited only weak, but still significant binding to pre-miR-30 (Figure 1B, lanes 11–15). The binding of the Exp5 orthologues to

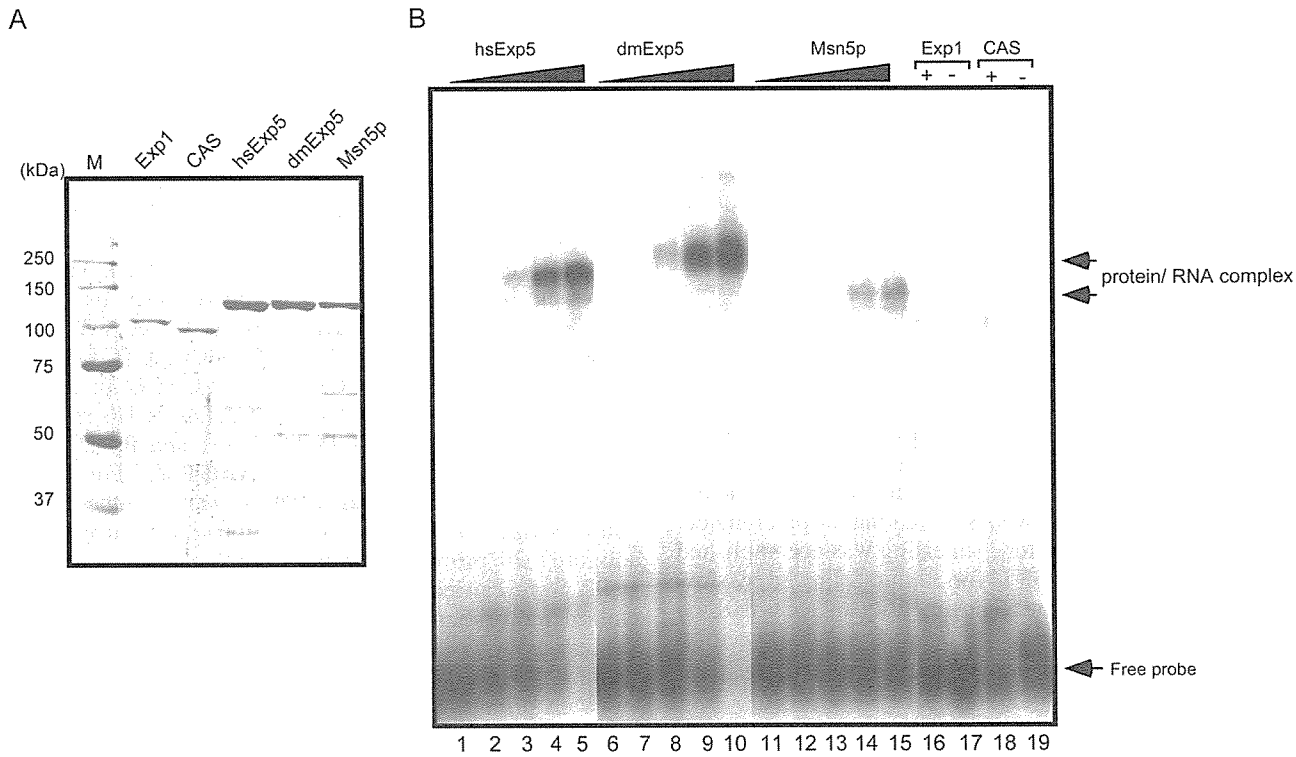

Figure 1. *In vitro* binding of the Exp5 orthologues to miRNA (**A**) The exportins indicated in each lane were expressed in *E.coli* and purified as indicated in Materials and Methods. After separation by SDS–PAGE, they were visualized by Coomassie blue staining. The positions of molecular weight markers are indicated in the left in kilo Daltons. (**B**) Binding of purified recombinant hsExp5 (lanes 1–5), dmExp5 (lanes 6–10) or Msn5p (lanes 11–15) to pre-miRNA was examined by EMSA. In the presence of 2 μM of hsRanQ69L-GTP (lanes 1– 5, 16, 18) or its orthologous mutants from cognate species (dmRanQ69L-GTP, lanes 6–10; yeast gsp1pQ71L-GTP, lanes 11–15), 0.07 (lanes 1, 6 and 11), 0.35 (lanes 2, 7 and 12), 0.7 (lanes 3, 8 and 13), 3.5 (lanes 4, 9 and14) and 7 (lanes 5, 10 and 15) pmol of each exportin was mixed up with radio-labeled pre-miR-30 probe. The migration of the probe was visualized by 6% non-denaturing PAGE followed by autoradiography. The positions of free and bound probe are indicated on the right. Purified Exp1 (lanes 16 and 17) and CAS (lanes 18 and 19) (7 pmol each) were also subjected to binding reactions as described above in the presence (+) (lanes 16 and 18) or absence (−) (lanes 17 and 19) of hsRanQ69L-GTP.

pre-miRNA was specific, since it was Ran-dependent (Figure 2A, lanes 1, 15 and 29) and no interaction between pre-miR-30 and CAS or Exp1, which are exportins for importin-α or leucine-rich NES-containing proteins, was detected irrespective of the presence of Ran-GTP (Figure 1B, lanes 16–19).

To further examine the specificity of the interactions between the Exp5 orthologues and pre-miRNA observed in Figure 1B, competition experiments were performed. Figure 2A indicates that unlabeled pre-miR-30 competed with labeled pre-miR-30 for binding to dmExp5 in a dose-dependent manner and as efficiently as that of hsExp5 (see also Figure 2B for quantitative data). From these data, we conclude that both hsExp5 and dmExp5 bind pre-miR-30 with similar efficiency.

On the other hand, as expected from the result shown in Figure 1B, unlabeled pre-miR-30 was a weak competitor for the binding of Msn5p to pre-miR-30. In contrast, we found that the interactions of all of the Exp5 orthologues to pre-miR-30 were efficiently inhibited by a 22 bp double-stranded (ds) RNA with a 2 nt overhang at the 3′-end (Figure 2A, lanes 11–14, 25–28 and 39–40), but not by a dsDNA encoding the same sequence (Figure 2A, lanes 7–10, 21–24 and 35–38). Interestingly, the binding of Msn5p to pre-miR-30, but not those of hsExp5 and dmExp5, was more efficiently competed with the shorter 22 bp dsRNA than with the miRNA precursor (Figure 2A, compare lanes 30–34 with lanes 39–42). To determine whether Msn5p recognizes the terminal structure of the dsRNA as a binding site, the inhibitory activity of another dsRNA that had the same sequence at double-stranded region with a 2 nt overhang at the 5′ end was tested (Figure 2C, bottom). The interaction between pre-miR-30 and hsExp5 or Msn5p was competed by the dsRNA with 3′ overhang, but not by that with 5′ overhang (Figure 2C, top). These results indicate that Msn5p specifically recognizes the terminal structure of the short dsRNA as reported for mammalian Exp5 (8,12). Thus, we conclude that the RNA binding activities of the Exp5 orthologues are evolutionary conserved from humans to budding yeast, but that there are significant differences in their substrate preferences.

dmExp5 binds tRNAs more strongly than does hsExp5

We next attempted to confirm the binding between labeled pre-miR-30 and Exp5 using *in vitro* translated proteins by a rabbit reticulocyte lysate (Figure 3A, left panel). As shown in Figure 3A right panel, lane 2, a retard band containing hsExp5 and pre-miR-30 was clearly observed. However, we found that *in vitro* translated dmExp5 did not bind pre-miR-30 under the same binding conditions (Figure 3A, right panel, lane 4). The same result was obtained when the

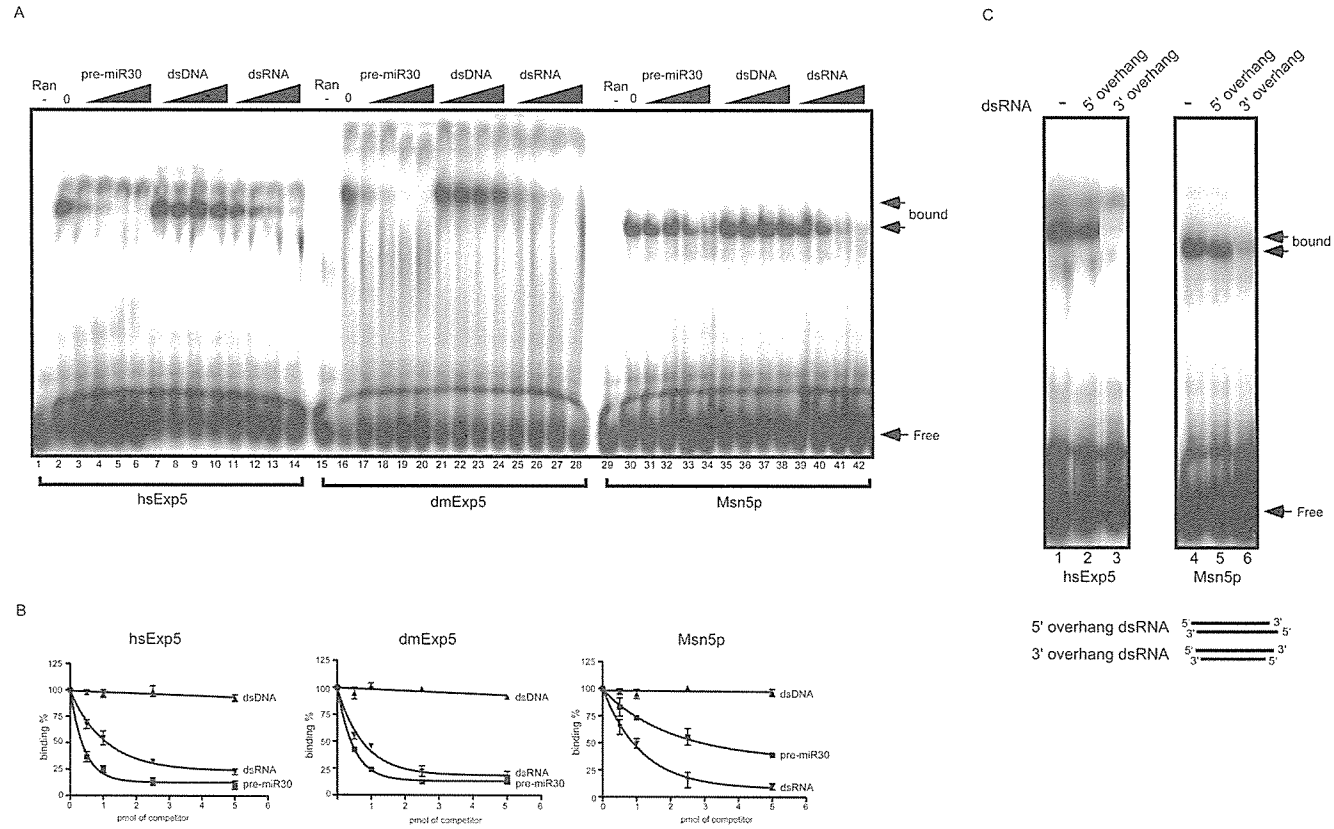

Figure 2. Binding specificities of the Exp5 orthologues. (**A**) Interaction between radio-labeled pre-miR-30 and hsExp5 (0.07 μM, lanes 1–14), dmExp5 (0.07 μM, lanes 15–28) or Msn5p (0.21 μM, lanes 29–42) in the presence (lanes 2–14, 16–28 and 30–42) or absence (lanes 1, 15 and 29) of hsRanQ69L-GTP or its orthologous mutants from cognate species was tested as in Figure 1. The binding reactions were performed in the presence of 0.5, 1, 2.5 or 5 pmol of the indicated competitors (unlabeled pre-miRNA, lanes 3–6, 17–20, 31–34; unlabeled dsDNA, lanes 7–10, 21–24, 35–38; unlabeled dsRNA, lanes 11–14, 25–28, 39–42). (**B**) Radio-activities co-migrating with the shifted bands were quantified using a phosphorimager. The values obtained without competitors were arbitrary set at 100 and those obtained with the indicated amounts of each competitor were calculated. Data are represented by means + SD of three independent experiments. (**C**) The binding of hsExp5 (lanes 1–3) or Msn5p (lanes 4–6) to radio-labeled pre-miR-30 is competed by 2.5 pmol of dsRNAs with the 5′ (lanes 2 and 5) or 3′ (lanes 3 and 6) protruding ends. The structures of dsRNAs are schematically indicated below the panel. In lanes 1 and 4, the binding reactions were performed without the unlabeled competitors. Arrows indicate the positions of free and bound probe.

bacterially expressed recombinant dmExp5 was incubated with pre-miR-30 in the presence of a rabbit reticulocyte lysate (Figure 3B, lane 3). These results raise the possibility that the reticulocyte lysate contains an activity that inhibits the binding between pre-miR-30 and dmExp5. Since the rabbit reticulocyte lysate contains a large amount of RNAs, including tRNAs, we explored the issue of whether the RNA fraction extracted from the reticulocyte lysate inhibits the binding between dmExp5 and pre-miR-30. As shown in Figure 3C, dmExp5 did not bind pre-miR-30 in the presence of the RNA fraction (compare lane 3 with 4). On the other hand, the binding of hsExp5 to pre-miRNA was unaffected under the same conditions (Figure 3B, lane 1 and 3C, lane 1).

To identify RNAs that cause the inhibition of binding between dmExp5 and pre-miR-30, dmExp5 expressed in *E.coli* as a histidine-tagged fusion protein (Figure 1B) was mixed with the rabbit reticulocyte lysate and immunoprecipitated with an anti-penta-His antibody. The co-precipitated RNAs were visualized by denaturing acrylamide gel electrophoresis followed by ethidium bromide staining. The bacterially expressed recombinant dmExp5 immunoprecipitated tRNAs only in the presence of dmRanQ69L-GTP (Figure 3D). Although the ability to bind tRNAs is conserved among the Exp5 orthologues from different species, we noticed that dmExp5 was able to immunoprecipitate the greatest amount of tRNAs among them. On the other hand, exportin-1 (Exp1) did not bind tRNAs at all.

To directly confirm that tRNAs actually inhibit the binding of dmExp5 to pre-miR-30, competition experiments were performed. Purified tRNA-Phe from baker's yeast inhibited dmExp5 from interacting with pre-miR-30 in a dose-dependent manner (Figure 4, upper panel, lanes 2–5), whereas negligible competition was found for binding between pre-miR-30 and hsExp5 (Figure 4, upper panel, lanes 10–14). Only a marginal effect was observed when U1ΔsmRNA was used as a competitor (Figure 4, upper panel, lanes 6–9). From these results, we conclude that dmExp5 preferentially binds to tRNA compared with hsExp5.

Knockdown of dmExp5 in Drosophila S2 cells decreases the amounts of tRNA and miRNA

Having established that dmExp5 fulfils the functional characteristics as an exportin for both miRNA and tRNA, we then examined whether dmExp5 functions as a sole exportin for both tRNAs and miRNAs in *Drosophila* cells. For this, we

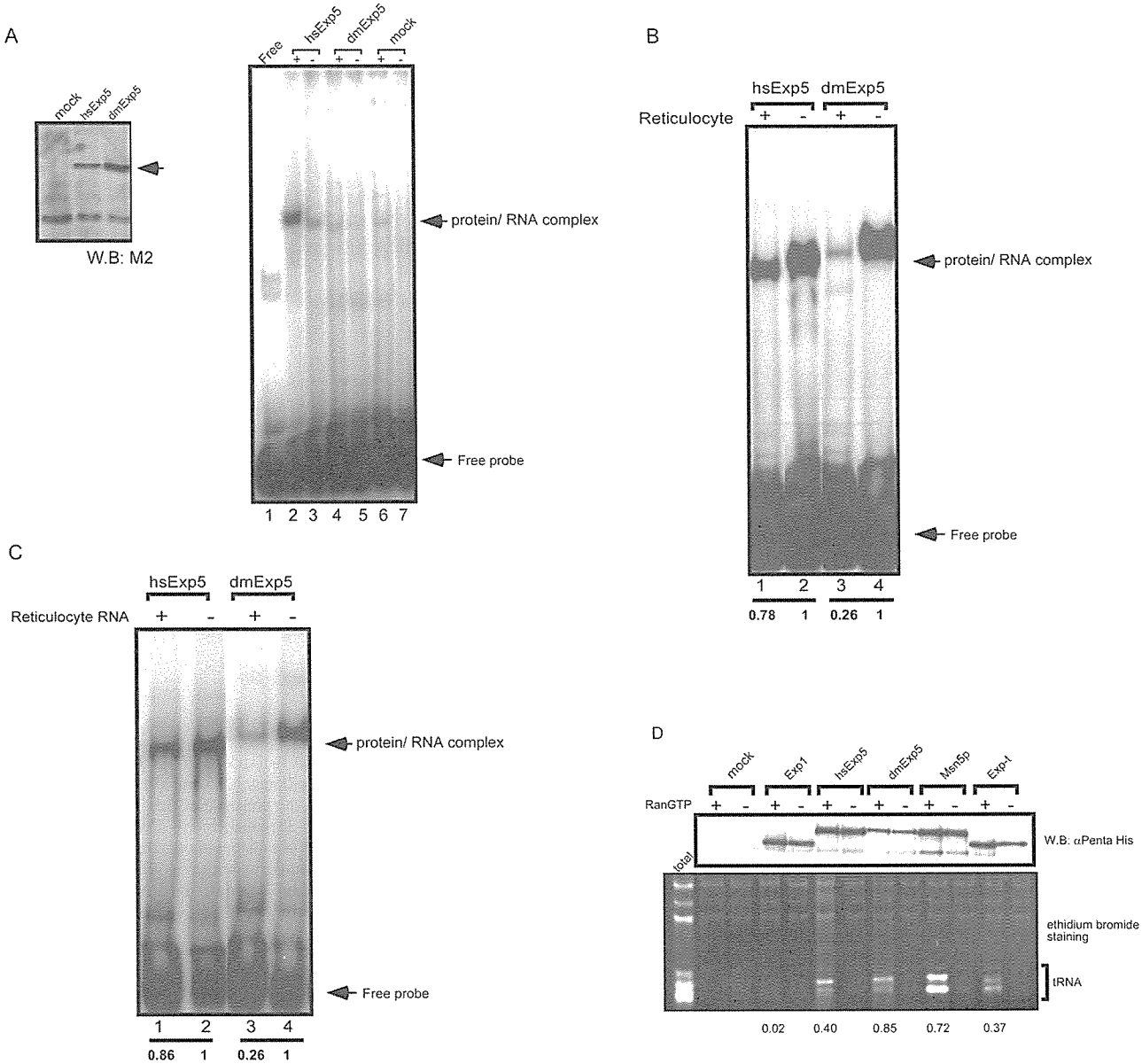

Figure 3. tRNA is a potent inhibitor of the interaction between pre-miR-30 and dmExp5. (**A**) *In vitro* translated hsExp5, but not dmExp5, bound pre-miR-30. Left panel: Expression of FLAG-tagged hsExp5 (lane 2) and dmExp5 (lane 3) using an *in vitro* translation system was confirmed by western blot using anti-FLAG antibody. In lane 1 (mock), an *in vitro* translation reaction programmed with an empty vector was loaded. Right panel: *In vitro* translated hsExp5 or dmExp5 as indicated in the left panel was mixed with radio-labeled pre-miR-30 in the presence (+, lanes 2, 4 and 6) or absence (−, lanes 3, 5 and 7) of hsRanQ69L-GTP (lanes 2 and 6) or dmRanQ69L-GTP (lane 4). The RNA–protein complex was detected by EMSA. In lane 1, radio-labeled pre-miR-30 alone was loaded. Arrows indicate the positions of bound and free probe. (**B**) Bacterially expressed recombinant dmExp5 failed to bind pre-miR-30 in the presence of a reticulocyte lysate. Bacterially expressed recombinant hsExp5 (lanes 1 and 2) or dmExp5 (lanes 3 and 4) along with RanQ69L-GTP were mixed with radio-labeled pre-miR-30 in the presence (indicated by +, lanes 1 and 3) or absence (indicated by −, lanes 2 and 4) of a reticulocyte lysate. The RNA-protein complexes were detected by EMSA. Arrows indicate the positions of bound and free probe. A quantification of the shifted bands was done by using a phosphor imager. The values obtained without the competitor were arbitrary set at 1 and those obtained with the competitor were calculated. The data are indicated below each lane. (**C**) The binding of dmExp5 to pre-miR-30 was inhibited by RNAs extracted from reticulocyte lysate. Bacterially expressed recombinant hsExp5 (lanes 1 and 2) or dmExp5 (lanes 3 and 4) along with RanQ69L-GTP were mixed with radio-labeled pre-miR-30 in the presence (lanes 1 and 3) or absence (lanes 2 and 4) of an RNA fraction isolated from reticulocyte lysate. The RNA–protein complexes were detected by EMSA. Arrows indicate the positions of bound and free probe. A quantification of the shifted bands was done as in (B). The data are indicated below each lane. (**D**) Co-immunoprecipitation of tRNAs with exportins. Bacterially expressed recombinant exportins indicated in each lane were mixed with a rabbit reticulocyte lysate in the presence (+) or absence (−) of RanQ69L-GTP or its orthologous mutants from cognate species. After immunoprecipitation with anti-pentaHis antibody-bound Protein G Sepharose, co-precipitated RNAs were extracted from the immunepellets and analyzed by denaturing PAGE followed by ethidium bromide staining (lower panel). Background binding was also examined in the absence of exportins (mock). Co-precipitated proteins were also detected by western blot using an anti-pentaHis antibody (upper panel). Ten percent of input was loaded on the left most lane (total). The amounts of the precipitated exportins and tRNAs in the presence of Ran-GTP were determined by densitometric scanning of the blot and the gel. The relative amounts of co-precipitated tRNAs, which are normalized to the amounts of each exportin, are indicated below the panel.

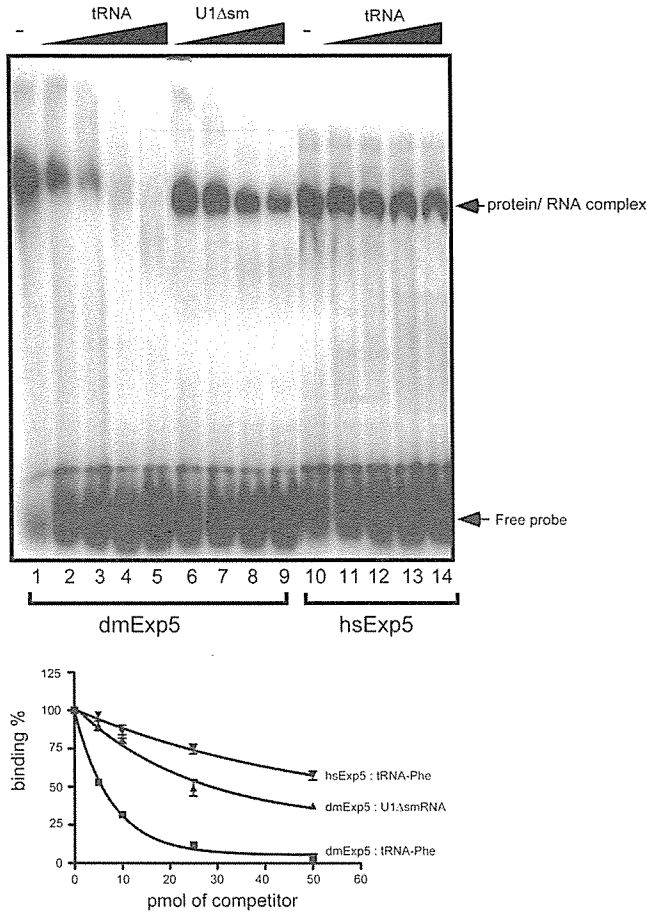

Figure 4. dmExp5 binds tRNA more preferentially than hsExp5. Upper panel: Bacterially expressed dmExp5 (lanes 1–9) or hsExp5 (lanes 10–14) were mixed with radio-labeled pre-miR-30 and RanQ69L-GTP orthologues from cognate species in the absence (lanes 1 and 10) or presence of 5 pmol (lanes 2, 6 and 11), 10 pmol (lanes 3, 7 and 12), 25 pmol (lanes 4, 8 and 13) or 50 pmol (lanes 5, 9 and 14) of indicated competitor RNAs. Protein–RNA complexes were detected by EMSA. Arrows indicate the positions of bound and free probe. Lower panel: Binding efficiency was calculated as in Figure 2B. Data are represented by means + SD of three independent experiments. Note that the concentrations of competitor RNAs were 10 times higher than those in Figure 2.

inactivated dmExp5 by RNAi-mediated gene silencing and measured the amounts of mature tRNA and miRNA, which we took for an indirect indication for their export defect as reported previously (8,9,32). As shown in Figure 5, the knockdown of dmExp5 in *Drosophila* S2 cells was confirmed by RT–PCR (Figure 5B, left panels). A significant decrease in tRNA-Met and tRNA-Ser as well as miR-2 levels was observed by the knockdown of dmExp5 (Figure 5B, right panels). On the contrary, upon depletion of hsExp5 in 293F cells, which was confirmed by a western blot (Figure 5A, left panels), the amounts of tRNA-Met and tRNA-Ser remained unaffected, whereas a significant decrease in mature let-7a was observed (Figure 5A, right panels) as reported previously (9). In both experiments, the amounts of U6 snRNA and U1 snRNA were not altered. In addition, as shown in Figure 5C, depletion of dmDGCR8 or dmDrosha (left panels), which are known components of the nuclear pri-miRNA processing complex, led to a significant decrease in the amount of mature miR-2. However, only marginal effects in tRNA levels were observed in these cells (Figure 5C, lanes 3 and 4). These findings exclude the possibility that the repression of tRNA caused by the depletion of dmExp5 in S2 cells was a secondary effect due to the loss of miRNA function. From these results, we conclude that dmExp5 plays important roles, not only in miRNA expression, but also in tRNA expression *in vivo*.

To further test if the observed effects by dmExp5 depletion could be rescued by hsExp5, complementation experiments were performed using S2 cells stably expressing FLAG-tagged hsExp5 (S2/hsExp5). S2 cells stably transfected with an empty vector (S2/Emp) served as a negative control. The knockdown of dmExp5 was checked by RT–PCR (Figure 6A, upper and middle panels), while the expression of hsExp5 was confirmed by western blot using an anti-FLAG antibody (Figure 6A, lower panel). In the S2/Emp, the amounts of miR-2 and tRNA-Ser decreased to 34 and 66% of the control level, respectively (lane 2 of Figure 6B top and middle panels). In contrast, when RNAi against dmExp5 was performed in S2/hsExp5, the amount of miR-2- decreased but to a much lower extent (68% of the control cells) (Figure 6B, top panel, right most lane), indicating that exogenously expressed hsExp5 significantly rescued the expression of pre-miRNA. In the same cells, the expression of tRNA-Ser was not rescued so efficiently (Figure 6B, middle panel). Unfortunately, a direct comparison between hsExp5 and hsExp-t could not be done, since we failed to obtain stable transformants of S2 cells that express sufficient amounts of hsExp-t (data not shown). These results indicate that the activity of dmExp5 is at least partially substituted by the expression of hsExp5 and that dmExp5 and hsExp5 are distinctly involved in the expression of pre-miRNA and tRNA.

DISCUSSION

In this study, three Exp5 orthologues from different species were extensively characterized. We found that, although the dsRNA binding abilities are well conserved from the budding yeast to human orthologues, certain differences exist in their optimal substrates. Msn5p binds the shorter dsRNA more efficiently than the longer hairpin like RNA (e.g. pre-miR-30), which was found to be the optimal substrate for human and fruit fly Exp5 by others as well as ourselves. In addition, recent studies have shown that, in plant *Arabidopsis*, miRNAs are detected as fully matured ~22 nt single stranded RNAs in both the nuclear and cytoplasmic fractions (32,37), indicating that HASTY, the *Arabidopsis* Exp5 orthologue, likely recognizes such short RNAs as cargoes (32). HASTY might inherit the observed substrate preference of yeast Msn5p, leading to the recognition of ~22 nt duplex RNAs as cargoes. These results suggest that the Exp5 orthologues have evolved different modes of substrate recognition to play different functional roles.

In vertebrates and plants, Exp5 is thought to act as a major exportin for pre-miRNAs and to play a minor role in the nuclear export of tRNAs. Consistent with this, we found that hsExp5 bound pre-miRNAs more efficiently than tRNAs and that the depletion of hsExp5 in human cells resulted in defects in miRNA but not in tRNA expression.

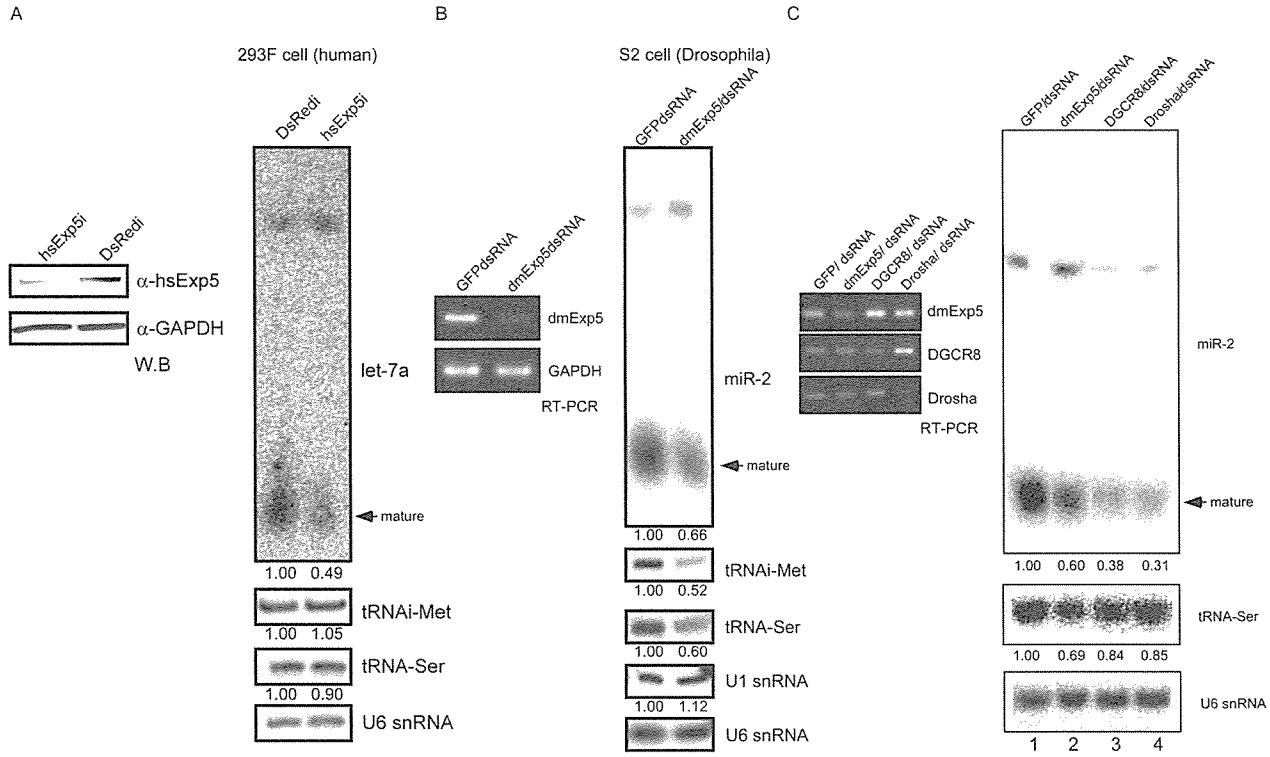

Figure 5. Knockdown of Exp5 in human and Drosophila cultured cells. (**A**) Let-7a, but not tRNAs, was depleted upon the knock down of hsExp5. Left panels: Human 293F cells were treated with siRNA against DsRed (DsRedi, which was used as a negative control) or hsExp5 (hsExp5i) for three days. The expression of hsExp5 in the cells was confirmed by western blot using anti-hsExp5 antibody (upper panel). The expression of GAPDH was detected as a control (lower panel). Right panels: Total RNAs were extracted from the siRNA treated cells. Northern blot analysis was performed using specific probes indicated on the right of each panel. The signal intensities were quantified by a phosphorimager and normalized by those of U6 snRNA. The relative expression level of each RNA was indicated below each panel. (**B**) Both miR-2 and tRNA were depleted upon dmExp5 knockdown. Left panels: *Drosophila* S2 cells were treated with 74 nM of the indicated dsRNA. Total RNAs were isolated 6 days later. GFP/dsRNA was used as a negative control. Expression of dmExp5 and GAPDH was confirmed by RT–PCR (upper panel). The amount of dmExp5 mRNA but not that of GAPDH was decreased upon dmExp5 depletion (lower panel). Right panels: Northern blot analysis was performed as in (A). Both miR-2 and tRNA levels were decreased by dmExp5 knockdown. (**C**) The amount of tRNAs was unaffected when miRNA processing factors were depleted. Left panels: S2 cells were treated with the indicated dsRNAs for four days. The knockdown of the expression of each mRNA was confirmed by RT–PCR. Right panels: Northern blot analysis was performed as in (A). Decrease in tRNA-Ser level was observed only when dmExp5 was knocked down.

On the other hand, it was reported that a decrease in tRNA levels, but not in miRNA levels, was observed in the *Arabidopsis* HASTY mutant, whereas the PAUSED mutation, which is the Exp-t orthologue of *Arabidopsis,* interfered with tRNA-Tyr processing without obvious effects on miRNA levels (32). In contrast, a previous report indicated that *Drosophila* does not posses an apparent orthologue of Exp-t (33). Despite repeated efforts, we also failed to identify the Exp-t gene in the *Apis mellifera* and *Anopheles gambiae* genomes. On the other hand, a putative Exp-t orthologue, designated as importin-β family 6 (Imb-6; GenBank accession NM_068919), was identified in the *C. elegans* genome. Thus, we speculate that the Exp-t gene might have been lost when the coelomata diverged from the bilateria. Instead, the following experimental evidence supports the notion that dmExp5 may have evolved as a substitute for the Exp-t function in such organisms. We demonstrated here that the depletion of dmExp5 in S2 cells induced the down regulation of both miRNAs and tRNAs and that dmExp5 binds tRNA with a higher affinity than hsExp5. From these results, we conclude that dmExp5, different from the other Exp5 orthologues, functions as a major export factor in the nuclear export of tRNAs as well as miRNAs in the fruit fly.

In budding yeast cells, Msn5p is known to be involved in the nuclear export of both tRNAs and a subset of proteins. Our *in vitro* binding data indicate that Msn5p is able to directly recognize RNAs. On the other hand, NESs of the protein cargoes recognized by Msn5p still remain unknown (13–18). Does Msn5p recognize both peptide sequences (or protein structure) and RNAs directly? As far as we know, there is no precedent for such a dual specificity in the importin-β family proteins. What common structural feature(s) in the different cargoes, then, can be recognized as NES by Msn5p? Of note in this context are the recent reports showing that, in mammalian cells JAZ and Staufen, dsRNA binding proteins involved in mRNA metabolism, are indirectly recognized by Exp5 via their affinities to small dsRNAs (38,39). To recognize the protein cargoes, mammalian Exp5 exploits dsRNAs as bridging factors. In yeast, Crz1p, which is functionally homologous to NFATs derived from higher eukaryotes, was reported to be exported by Msn5p (14). Because it was recently demonstrated that an ncRNA is involved in the nuclear localization of mammalian NFATs (40,41), it is conceivable that NFATs have the ability to bind directly or indirectly RNAs. Therefore, it would be very tempting to speculate that Msn5p, via its affinity to

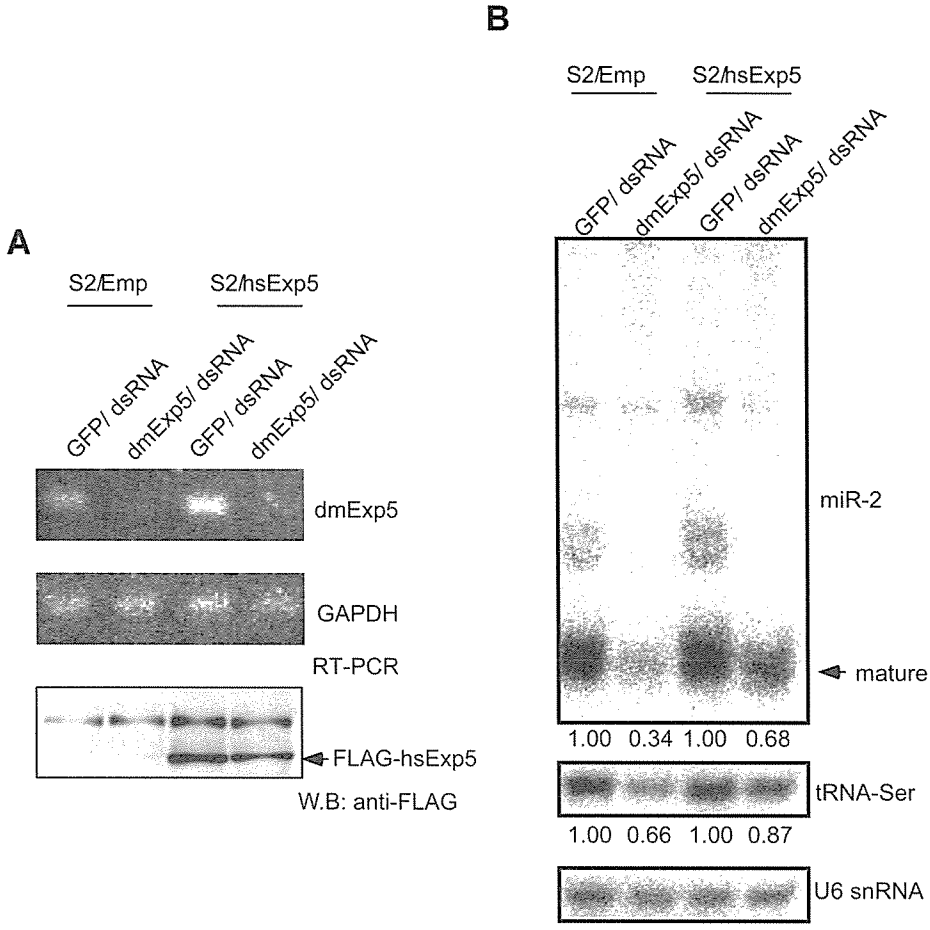

Figure 6. The repression of miRNA and tRNA levels induced by knockdown of dmExp5 was restored by overexpression of hsExp5. S2/hsExp5, a S2 cell derivative stably expressing hsExp5, was treated with 111 nM of the indicated dsRNAs as described in Figure 6B. S2/Emp, which harbors an empty vector, was used as a negative control. $CuSO_4$ was added to the culture media 24 h after dsRNA treatment (see Materials and Methods). (**A**) Depletion of dmExp5 was confirmed by RT–PCR (upper and middle panels). Expression of hsExp5 was confirmed by western blot using anti-FLAG M2 antibody (lower panel). (**B**) Northern blot analysis was performed as described in Figure 6A. The repression of miRNA and tRNA induced by knockdown of dmExp5 was partially restored by the expression of hsExp5.

small dsRNAs, indirectly recognizes the protein cargoes. Recent genome wide transcription profiling studies suggest that a large proportion of the genome including intergenic regions, is transcribed in both directions in various organisms. These observations indicate that the expression of non-coding RNAs and possibly dsRNAs is more widespread in eukaryotic cells than has ever been expected (42–44). Further experiments will be required to determine whether such bridging dsRNAs do exist.

ACKNOWLEDGEMENTS

We thank Drs Mutsuhito Ohno (Kyoto University) and Tohru Yoshihisa (Nagoya University) for providing various plasmids. This work was supported, in part, by grants from the Japanese Ministry of Education, Culture, Sports, Science and Technology and the Human Frontier Science Program. Funding to pay the Open Access publication charges for this article was provided by Japanese Ministry of Education, Culture, Sports, Science and Technology (MEXT).

Conflict of interest statement. None declared.

REFERENCES

1. Chook,Y.M. and Blobel,G. (2001) Karyopherins and nuclear import. *Curr. Opin. Struct. Biol.*, **11**, 703–715.
2. Kuersten,S., Ohno,M. and Mattaj,I.W. (2001) Nucleocytoplasmic transport: Ran, beta and beyond. *Trends Cell Biol.*, **11**, 497–503.
3. Quimby,B.B. and Corbett,A.H. (2001) Nuclear transport mechanisms. *Cell Mol. Life Sci.*, **58**, 1766–1773.
4. Weis,K. (2002) Nucleocytoplasmic transport: cargo trafficking across the border. *Curr. Opin. Cell Biol.*, **14**, 328–335.
5. Izaurralde,E., Kutay,U., von Kobbe,C., Mattaj,I.W. and Gorlich,D. (1997) The asymmetric distribution of the constituents of the Ran system is essential for transport into and out of the nucleus. *EMBO J.*, **16**, 6535–6547.
6. Yoneda,Y., Hieda,M., Nagoshi,E. and Miyamoto,Y. (1999) Nucleocytoplasmic protein transport and recycling of Ran. *Cell Struct. Funct.*, **24**, 425–433.
7. Bohnsack,M.T., Czaplinski,K. and Gorlich,D. (2004) Exportin 5 is a RanGTP-dependent dsRNA-binding protein that mediates nuclear export of pre-miRNAs. *RNA*, **10**, 185–191.
8. Lund,E., Guttinger,S., Calado,A., Dahlberg,J.E. and Kutay,U. (2004) Nuclear export of microRNA precursors. *Science*, **303**, 95–98.
9. Yi,R., Qin,Y., Macara,I.G. and Cullen,B.R. (2003) Exportin-5 mediates the nuclear export of pre-microRNAs and short hairpin RNAs. *Genes Dev.*, **17**, 3011–3016.
10. Gwizdek,C., Ossareh-Nazari,B., Brownawell,A.M., Evers,S., Macara,I.G. and Dargemont,C. (2004) Minihelix-containing RNAs

mediate exportin-5-dependent nuclear export of the double-stranded RNA-binding protein ILF3. *J. Biol. Chem.*, **279**, 884–891.
11. Gwizdek,C., Ossareh-Nazari,B., Brownawell,A.M., Doglio,A., Bertrand,E., Macara,I.G. and Dargemont,C. (2003) Exportin-5 mediates nuclear export of minihelix-containing RNAs. *J. Biol. Chem.*, **278**, 5505–5508.
12. Zeng,Y. and Cullen,B.R. (2004) Structural requirements for pre-microRNA binding and nuclear export by Exportin 5. *Nucleic Acids Res.*, **32**, 4776–4785.
13. Blondel,M., Alepuz,P.M., Huang,L.S., Shaham,S., Ammerer,G. and Peter,M. (1999) Nuclear export of Far1p in response to pheromones requires the export receptor Msn5p/Ste21p. *Genes Dev.*, **13**, 2284–2300.
14. Boustany,L.M. and Cyert,M.S. (2002) Calcineurin-dependent regulation of Crz1p nuclear export requires Msn5p and a conserved calcineurin docking site. *Genes Dev.*, **16**, 608–619.
15. DeVit,M.J. and Johnston,M. (1999) The nuclear exportin Msn5 is required for nuclear export of the Mig1 glucose repressor of *Saccharomyces cerevisiae*. *Curr. Biol.*, **9**, 1231–1241.
16. Kaffman,A., Rank,N.M., O'Neill,E.M., Huang,L.S. and O'Shea,E.K. (1998) The receptor Msn5 exports the phosphorylated transcription factor Pho4 out of the nucleus. *Nature*, **396**, 482–486.
17. Queralt,E. and Igual,J.C. (2003) Cell cycle activation of the Swi6p transcription factor is linked to nucleocytoplasmic shuttling. *Mol. Cell. Biol.*, **23**, 3126–3140.
18. Yoshida,K. and Blobel,G. (2001) The karyopherin Kap142p/Msn5p mediates nuclear import and nuclear export of different cargo proteins. *J. Cell Biol.*, **152**, 729–740.
19. Takano,A., Endo,T. and Yoshihisa,T. (2005) tRNA actively shuttles between the nucleus and cytosol in yeast. *Science*, **309**, 140–142.
20. Arts,G.J., Kuersten,S., Romby,P., Ehresmann,B. and Mattaj,I.W. (1998) The role of exportin-t in selective nuclear export of mature tRNAs. *EMBO J.*, **17**, 7430–7441.
21. Arts,G.J., Fornerod,M. and Mattaj,I.W. (1998) Identification of a nuclear export receptor for tRNA. *Curr. Biol.*, **8**, 305–314.
22. Kutay,U., Lipowsky,G., Izaurralde,E., Bischoff,F.R., Schwarzmaier,P., Hartmann,E. and Gorlich,D. (1998) Identification of a tRNA-specific nuclear export receptor. *Mol. Cell*, **1**, 359–369.
23. Lipowsky,G., Bischoff,F.R., Izaurralde,E., Kutay,U., Schafer,S., Gross,H.J., Beier,H. and Gorlich,D. (1999) Coordination of tRNA nuclear export with processing of tRNA. *RNA*, **5**, 539–549.
24. Hellmuth,K., Lau,D.M., Bischoff,F.R., Kunzler,M., Hurt,E. and Simos,G. (1998) Yeast Los1p has properties of an exportin-like nucleocytoplasmic transport factor for tRNA. *Mol. Cell. Biol.*, **18**, 6374–6386.
25. Sarkar,S. and Hopper,A.K. (1998) tRNA nuclear export in *Saccharomyces cerevisiae*: *in situ* hybridization analysis. *Mol. Biol. Cell*, **9**, 3041–3055.
26. Grosshans,H., Hurt,E. and Simos,G. (2000) An aminoacylation-dependent nuclear tRNA export pathway in yeast. *Genes Dev.*, **14**, 830–840.
27. Calado,A., Treichel,N., Muller,E.C., Otto,A. and Kutay,U. (2002) Exportin-5-mediated nuclear export of eukaryotic elongation factor 1A and tRNA. *EMBO J.*, **21**, 6216–6224.
28. Bohnsack,M.T., Regener,K., Schwappach,B., Saffrich,R., Paraskeva,E., Hartmann,E. and Gorlich,D. (2002) Exp5 exports eEF1A via tRNA from nuclei and synergizes with other transport pathways to confine translation to the cytoplasm. *EMBO J.*, **21**, 6205–6215.
29. Bollman,K.M., Aukerman,M.J., Park,M.Y., Hunter,C., Berardini,T.Z. and Poethig,R.S. (2003) HASTY, the Arabidopsis ortholog of exportin 5/MSN5, regulates phase change and morphogenesis. *Development*, **130**, 1493–1504.
30. Hunter,C.A., Aukerman,M.J., Sun,H., Fokina,M. and Poethig,R.S. (2003) PAUSED encodes the Arabidopsis exportin-t ortholog. *Plant Physiol.*, **132**, 2135–2143.
31. Li,J. and Chen,X. (2003) PAUSED, a putative exportin-t, acts pleiotropically in Arabidopsis development but is dispensable for viability. *Plant Physiol.*, **132**, 1913–1924.
32. Park,M.Y., Wu,G., Gonzalez-Sulser,A., Vaucheret,H. and Poethig,R.S. (2005) Nuclear processing and export of microRNAs in Arabidopsis. *Proc. Natl Acad. Sci. USA*, **102**, 3691–3696.
33. Lippai,M., Tirian,L., Boros,I., Mihaly,J., Erdelyi,M., Belecz,I., Mathe,E., Posfai,J., Nagy,A., Udvardy,A. *et al.* (2000) The Ketel gene encodes a Drosophila homologue of importin-beta. *Genetics*, **156**, 1889–1900.
34. Kudo,N., Wolff,B., Sekimoto,T., Schreiner,E.P., Yoneda,Y., Yanagida,M., Horinouchi,S. and Yoshida,M. (1998) Leptomycin B inhibition of signal-mediated nuclear export by direct binding to CRM1. *Exp. Cell Res.*, **242**, 540–547.
35. Tachibana,T., Hieda,M., Miyamoto,Y., Kose,S., Imamoto,N. and Yoneda,Y. (2000) Recycling of importin alpha from the nucleus is suppressed by loss of RCC1 function in living mammalian cells. *Cell Struct. Funct.*, **25**, 115–123.
36. Clemens,J.C., Worby,C.A., Simonson-Leff,N., Muda,M., Maehama,T., Hemmings,B.A. and Dixon,J.E. (2000) Use of double-stranded RNA interference in Drosophila cell lines to dissect signal transduction pathways. *Proc. Natl Acad. Sci. USA*, **97**, 6499–6503.
37. Zhang,B., Pan,X., Cannon,C.H., Cobb,G.P. and Anderson,T.A. (2006) Conservation and divergence of plant microRNA genes. *Plant J.*, **46**, 243–259.
38. Chen,T., Brownawell,A.M. and Macara,I.G. (2004) Nucleocytoplasmic shuttling of JAZ, a new cargo protein for exportin-5. *Mol. Cell. Biol.*, **24**, 6608–6619.
39. Macchi,P., Brownawell,A.M., Grunewald,B., DesGroseillers,L., Macara,I.G. and Kiebler,M.A. (2004) The brain-specific double-stranded RNA-binding protein Staufen2: nucleolar accumulation and isoform-specific exportin-5-dependent export. *J. Biol. Chem.*, **279**, 31440–31444.
40. Mattick,J.S. (2005) The functional genomics of noncoding RNA. *Science*, **309**, 1527–1528.
41. Willingham,A.T., Orth,A.P., Batalov,S., Peters,E.C., Wen,B.G., Aza-Blanc,P., Hogenesch,J.B. and Schultz,P.G. (2005) A strategy for probing the function of noncoding RNAs finds a repressor of NFAT. *Science*, **309**, 1570–1573.
42. Okazaki,Y., Furuno,M., Kasukawa,T., Adachi,J., Bono,H., Kondo,S., Nikaido,I., Osato,N., Saito,R., Suzuki,H. *et al.* (2002) Analysis of the mouse transcriptome based on functional annotation of 60,770 full-length cDNAs. *Nature*, **420**, 563–573.
43. Katayama,S., Tomaru,Y., Kasukawa,T., Waki,K., Nakanishi,M., Nakamura,M., Nishida,H., Yap,C.C., Suzuki,M., Kawai,J. *et al.* (2005) Antisense transcription in the mammalian transcriptome. *Science*, **309**, 1564–1566.
44. Carninci,P., Sandelin,A., Lenhard,B., Katayama,S., Shimokawa,K., Ponjavic,J., Semple,C.A., Taylor,M.S., Engstrom,P.G., Frith,M.C. *et al.* (2006) Genome-wide analysis of mammalian promoter architecture and evolution. *Nat. Genet.*, **38**, 626–635.